EVALUATION OF BIOPHYSICAL ASPECTS OF CANCER USING LAB-ON-A CHIP DEVICES

A Thesis Submitted to
the Graduate School of Engineering and Science of
İzmir Institute of Technology
in Partial Fulfillment of the Requirements for the Degree of

MASTER OF SCIENCE

in Biotechnology and Bioengineering

by
İsmail TAHMAZ

July 2019
İZMİR

We approve the thesis of **İsmail TAHMAZ**

Examining Committee Members:

Prof. Dr. Devrim PESEN OKVUR
Department of Molecular Biology and Genetic, İzmir Institute of Technology

Asst. Prof. Dr. Çiğdem TOSUN
Department of Molecular Biology and Genetic, İzmir Institute of Technology

Assoc. Prof. Dr. Şerif ŞENTÜRK
Department of Genome Science and Molecular Biotechnology & İzmir International Biomedicine and Genome Institute, Dokuz Eylül University

17 July 2019

Prof. Dr. Devrim PESEN OKVUR
Supervisor, Department of Molecular Biology and Genetic

Asst. Prof. Dr. Nur Başak SÜRMELİ
Co-Supervisor, Department of Biotechnology and Bioengineering

Assoc. Prof. Dr. Engin ÖZÇİVİCİ
Head of the Department of Biotechnology Bioengineering

Prof. Dr. Aysun SOFUOĞLU
Dean of the Graduated School of Engineering and Science

ACKNOWLEDGMENTS

I would like to thank my supervisor Prof. Dr. Devrim PESEN OKVUR for her guidance, trust and support throughout this study.

I would like to thank TUBITAK where finance this thesis with 1003 project which titled “115E057” coordinated by Assoc. Prof. Dr. Özden YALÇIN ÖZUYSAL and Assoc. Prof. Dr. Gülistan MEŞE ÖZÇİVİCİ and Assoc. Prof. Dr. Engin ÖZÇİVİCİ for permission to using fluorescence microscopes and Assist. Prof. Dr. Çiğdem TOSUN for precious immunofluorescence and any hypoxia related help for this study.

I would like to express my deepest appreciation to our team and alumni of the Controlled *in vitro* Microenvironments (C*iv*M) Laboratory for their support, especially Gizem BATI AYAZ and Müge BİLGEN for their remarkable contributions to this study, and Sevgi ÖNAL, Funda BİLGİLİ, Begüm GÖKÇE, Ali YETGİN, Ali CAN, Aslı KISIM, Deniz KANKALE, Abdurehman Eshete MOHAMMED, Nurullah SATI, Yeşim ŞİRİN, Derya USTA, Deniz Cemre TURGUT, Osman Halil SUBAY.

I owe to Burcu FIRATLIGIL YILDIRIR, Yağmur Ceren UNAL, Mustafa ILHAN, Hilal CİHANKAYA, Çağlar ÇİL, Gizem Tuğçe ULU, Kübra TELLİ, Fikrican DİLEK, Gözde YEŞİLTAŞ, Ceren TABAK BURU, Özge KARADAŞ, Deniz UĞUR, Melis OLÇUM, Asli ADAK as my collegues a debt of graditute for kindness and any other support

Finally, I would like to explain my appreciation and endless thanks to my family Cavit TAHMAZ, Ümmühan TAHMAZ, Çiğdem YANGIN, Ahmet Önder YANGIN, Tuğba YANGIN, Ceyda YANGIN and my best friends Cemil Efehan PALA, Tuğba DURMUŞOĞLU, Selda Nur ŞİMŞİR who all belongs to my family for their encouragement, understanding and support during my whole and academic life.

ABSTRACT

EVALUATION OF BIOPHYSICAL ASPECTS OF CANCER USING LAB-ON-A CHIP DEVICES

Breast cancer metastasis is really crucial point from cancer related deaths. As cancer cells from primary tumor are travelling through blood, they hang on to blood vessel and finally they exit from blood vessel into secondary site where is extracellular matrix and/or tissue/organ. This process commonly known as extravasation. Cancer cells sometimes can be highly aggressive when it exposed to hypoxia referred low oxygen amount by activating HIF1α. This transcription factor is activated in malignant cells, normal cells and endothelial cells in blood vessel when oxygen amount decreased to certain levels and it induce several genes expression such as VEGF, LOX, Angiopoietin-like-4 etc. In this study we investigated effect of HIF1α which is hypoxia indicator on breast cancer extravasation by comparing to normal oxygen level. This study represents both anemic hypoxia physiologically and lead to understand underlying mechanism of extravasation into extracellular matrix related to low oxygen circulating through blood. In addition to HIF1α effects, dynamic perfusion mimicking blood flow was applied to determine effects on extravasation. For this purpose, lab-on-a chip device was utilized for real time visualization. In conclusion, although hypoxia is giving permission MDAMB231 to extravasate because of reshaping of vascular geometry, less extravasated cancer cells observed in matrix during hypoxia under both static and flow condition when compared to normoxic and static conditions. Moreover, it was shown that flow triggers extravasation distance in normoxia against static condition and normal breast epithelial cells extravasated away in hypoxia comparing breast cancer cells by means of flow.

Keywords and Phrases: breast cancer, hypoxia, normoxia, metastasis, extravasation, microfluidics

ÖZET

KANSERİN BİYOFİZİKSEL YÖNLERİNİN YONGA-ÜSTÜ-LABORATUVAR AYGITLARI KULLANILARAK DEĞERLENDİRİLMESİ

Meme kanseri metastazı kanser ilişkili ölümlerden dolayı gerçekten çok önemlidir. Birincil tümörden gelen kanser hücreleri kan damarında dolaşırken kan damarına tutunur ve son olarak kan damarından hücre dışı matriks ve / veya doku / organ olan ikincil bölgeye çıkarlar. Bu süreç genellikle ekstravazasyon olarak bilinir. Kanser hücreleri düşük oksijen seviyesini temsil eden hipoksiye maruz kaldıklarında bazen HIF1α'yı aktive ederek oldukça saldırgan olabilirler. Bu transkripsiyon faktörü, oksijen miktarı belirli seviyelere düştüğünde hem kötü huylu hücrelerde, hem normal hücrelerde hem de kan damarının fizyolojik yapısında bulunan endotel hücrelerinde aktifleşir ve VEGF, LOX, Angiopoietin benzeri-4 gibi çeşitli genlerin ifadesini teşvik eder. Bu çalışmada hipoksi göstergesi HIF1α 'nın normal oksijen seviyesine göre meme kanseri ekstravazasyonu üzerine etkisini araştırdık. Bu çalışma hem anemik hipoksiyi fizyolojik olarak temsil etmekte hem de kanda dolaşan düşük oksijene bağlı hücre dışı matrikse ekstravazasyonun altında yatan mekanizmanın anlaşılmasına olanak vermektedir. HIF1α etkilerine ek olarak, ekstravazasyon üzerindeki etkilerin belirlenmesi için kan akışını taklit eden dinamik perfüzyon akışı uygulandı. Bu amaçla, gerçek zamanlı görüntüleme için yonga-üstü-laboratuvar aygıtı kullanıldı. Sonuç olarak, hipoksi damar geometrisini değiştirmesinden dolayı MDAMB231 hücrelerinin ekstravazasyonuna izin verse de, hipoksi sırasında normal oksijen seviyesi ve statik koşullara kıyasla hem statik hem de akış koşullarında matrikste daha az ekstravaze olan kanser hücresi gözlemledik. Ayrıca akışın, normal oksijen seviyesinde statik durum üzerinde ekstravazasyon mesafesini tetiklediği ve hipoksi durumunda meme kanseri hücrelerine kıyasla normal meme epitel hücrelerini akış yoluyla matrikste daha uzağa ekstravaze olduğu gösterilmiştir.

Anahtar Kelimeler: meme kanseri, hipoksi, normoksi, metastaz, ekstravazasyon, mikroakışkanlar

TABLE OF CONTENT

LIST OF FIGURES ix

CHAPTER 1 INTRODUCTION 1

1.1. Breast Cancer and Metastasis 1

1.2. Hypoxia, Physoxia and Normoxia 2

1.3. Energy Metabolism in Cells 2

1.4. HIF1α Mechanism and Simulation of Hypoxia 3

1.5. HIF1 Related Genes Responsible for Metastasis 4

1.6. Biophysical Aspects of Hypoxia and Related Terms for Physiology 5

1.7. Microfluidics and Lab-on-a chip Devices 6

1.8. Previous Literature Summary 6

1.9. Aim 7

CHAPTER 2 MATERIALS AND METHODS 8

2.1. Device Fabrication 8

2.2. Device Coating 12

2.3. Cell Lines Preparation and Tracking 12

2.4. Cell Loading and Gel Preparation 13

2.5. Flow Optimization 14

2.5. Endothelial Monolayer Integrity Assay 16

2.6. Cell Viability Assay 16

2.7. Determination of HIF1α Localization 18

2.8. Extravasated Cell Quantification and Extravasation Metric 19

2.9. Distance of Extravasated Cell Quantification 22

2.10. Statistical Analysis 23

CHAPTER 3 RESULTS 24

3.1. Effect of Cobalt Chloride on Cell Viabilities 24

3.2. Determination of HIF1α Localization 25

3.3. Effects of Coating and Cell Number on Endothelial Monolayer Formation 29

3.4. Permeability Assessment of Endothelial Monolayer during Hypoxia and Normoxia in Dynamic and Static Conditions 31

3.5. Extravasated Particle and Metric Quantification 35

3.6. Determination of Extravasated Cell Distance 39

CHAPTER 4 DISCUSSIONS 41

CHAPTER 5 CONCLUSION 43

REFERENCES 44

APPENDIX A SUPPLEMENTARY FIGURES 50

LIST OF FIGURES

Figure **Page**

Figure 2. 1. The pattern to be printed on the master mold with UV lithography. 10
Figure 2. 2. The master mold prepared with UV lithography.....10
Figure 2. 3. The state of the polymerized PDMS as a result of soft lithography after removal from master mold.....11
Figure 2. 4. A photo showing how to measure height of channel. 11
Figure 2. 5. An image representing loading and settling of endothelial cells for endothelial monolayer formation. a)loading of cells b)settling down of lab-on-a chip with cells in staining jar overnight.....14
Figure 2. 6. An image showing the height difference and length at the inlet and outlet according to angle set at the rotator for flow optimization.....15
Figure 2. 7. An image represents selected ROIs for endothelial monolayer integrity analysis. ROI-1 shows mean intensity in the gel region, ROI-4 is background intensity. Scale bar:100 um.....16
Figure 2. 8. Representative image indicating a) intact b) nonintact monolayer 20
Figure 2. 9. Representing image of extravasation. dashed circle: circulated cells in endothelial monolayer , straight circle: extravasated cells from endothelial monolayer. *=matrix, **=flow channel. Scale Bar: 200 μM.. 20
Figure 2. 10. The appearance of the extravasated cell outside (top) the endothelial monolayer and invisibleness (bottom) inside the endothelial monolayer green:endothelial cells, red: circulated cells. *=matrix,**=flow channel. Scale Bar: 200 μM......21
Figure 2. 11. Representing image of associated cells adjacent to endothelial monolayer boundry between monolayer and matrix. green: endothelial cells, red: circulated cells. *=matrix,**=flow channel. (endothelial cells sometimes can migrate to matrix). Scale Bar: 200 μM 21
Figure 2. 12. An image showing the brightfield, 488 and 555 fluorescence and merged channels for extravasation analysis in 2D. 22

Figure **Page**

Figure 2. 13. A photo showing the distance of the extravasated cell to the endothelial monolayer, which determines the outermost point of the endothelial monolayer and is extravasated in the same "z" position. green: endothelial monolayer, red: extravasated cell. *=matrix, **=flow channel (endothelial cell sometimes can migrate to matrix channel) 23
Figure 3. 1. Effects of $CoCl_2$ on cell viabilities seperately. *= p<0.05, **= p<0.01.....24
Figure 3. 2. Effects of $CoCl_2$ among each other. n.s=not significant 25
Figure 3. 3. Different doses of $CoCl_2$ on bEnd.3, MDAMB231, MCF10A viabilities for 24 hour. Scale bar: 100 µm.....25
Figure 3. 4. Image representing HIF1α localization in bEnd.3 nuclei at different time 26
Figure 3. 5. HIF1α localization in bEnd.3 nuclei at different time intervals with 100 µm $CoCl_2$ and without $CoCl_2$ (control) in terms of mean intensity of nuclei. ***= p<0.001.....27
Figure 3. 6. HIF1α localization in bEnd.3 nuclei at different time intervals with 100 µm $CoCl_2$ and without $CoCl_2$ (control) by searching any intensity in nuclei. *= p<0.05, ***= p<0.001 27
Figure 3. 7. HIF1α localization in bEnd.3 cells nuclei without $CoCl_2$ in 100x objective Scale bar: 100 µm.....28
Figure 3. 8. HIF1α localization in bEnd.3 cells nuclei with 100 µm $CoCl_2$ in 100x objective. Scale bar: 100 µm 28
Figure 3. 9. $20x10^6$ endothelial cell restructuring with poli-L-lysine and fibronectin coating prior to loading the cells in different positions 30
figure 3. 10. $20x10^6$ endothelial cell restructuring with APTES and fibronectin coating prior to loading the cells in different positions. Scale Bar: 200 µM 30
figure 3. 11. $7.5x10^6$ cell loading into device coated with various proteins at same concentrations. a)0.0125 mg/ml collagen type i b)0.0125 mg/ml fibronectin c) 0.0125 mg/ml laminin. Scale Bar: 200 µM 31
Figure 3. 12. Cell number trial for endothelial monolayer formation. a)110000 cells/ml, b) 1500000 cells/ml c)7500000 cells/ml. Scale Bar: 200 µM 31

Figure **Page**

Figure 3. 13. 70 kDa TMR dextran diffusion across endothelial monolayer at 1 and 30 minute under static condition. only matrigel=without endothelial monolayer . Scale bar: 100 μm 32
Figure 3. 14. 70 kDa TMR dextran diffusion across endothelial monolayer at 1 and 30 minute with 0.77 dyne/cm^2. only matrigel=without endothelial monolayer . Scale bar: 100 μm 33
Figure 3. 15. 70 kDa TMR dextran diffusion across endothelial monolayer to gel region at 1 minute normoxia, severe (4 hour) and mild (6 hour) hypoxia and without endothelial monolayer. ***=p<0.001 34
Figure 3. 16. 70 kDa TMR dextran diffusion across endothelial monolayer to gel region at 30 minutes normoxia, severe (4 hour) and mild (6 hour) hypoxia and without endothelial monolayer with perfusion flow and without perfusion flow ***=p<0.001 34
Figure 3. 17. Average extravasated cell number from intact endothelial monolayer. *=p<0.05 36
Figure 3. 18. Extravasation metric in intact endothelial monolayer. *=p<0.05 36
Figure 3. 19. Average extravasated cell number from intact and nonintact endothelial monolayer. *=p<0.05, **=p<0.01 37
Figure 3. 20. Extravasation metric in intact and nonintact endothelial monolayer. *=p<0.05, **=p<0.01 37
Figure 3. 21. Average extravasated and associated cell number from intact endothelial monolayer. *=p<0.05, **=p<0.01 38
Figure 3. 22. Average extravasated and associated cell number from intact and nonintact endothelial monolayer. *=p<0.05, **=p<0.01 38
Figure 3. 23. Extravasated cell distance across intact and nonintact endothelial monolayer *=p<0.05 40
Figure 3. 24. Extravasated cell distance across intact endothelial monolayer *=p<0.05, **=p<0.01 40

Figure **Page**

Figure A. 1. MDAMB231 and MCF10A viabilities when they preconditioned in non treated petri dish 100 µm $CoCl_2$ for 6 hour. (propidium iodide shows dead cells). Scale Bar= 100 µm.....50
Figure A. 2. An image showing HIF1α lozalization in nuclei of MDAMB231 and MCF10A when 100 µm $CoCl_2$ applied for 6 hour. Scale Bar= 100 µm. 51
Figure A. 3. State of circulated cells to be loaded into flow channel for observing extravasation event. a)10000 cells/ml b)20000 cells/ml. Scale Bar: 200 µm.....51
Figure A. 4. Top view of endothelial monolayer without 8%450-650 kDa dextran. Scale Bar: 200 µm.....52
Figure A. 5. Top view of endothelial monolayer with 8%450-650 kDa dextran. Scale Bar: 200 µm.....52
Figure A. 6. Excel sheet showing shear stress calculation based on height, flow rate and height differences between inlet and outlet according to degree entered.....53
Figure A. 7. Effect of 100 µm $CoCl_2$ treatment against MDAMB231 morphology. Scale Bar: 100µm.....53
Figure A. 8. Observation of tumor formation on 5th and 10th day. Scale Bar: 200 µm 54
Figure A. 9. Excel sheet showing extravasated, associated and total cells in flow channel according to hypoxic and normoxic situations without perfusion flow. green bar:intact monolayer, orange bar: nonintact monolayer.....55

CHAPTER 1

INTRODUCTION

1.1. Breast Cancer and Metastasis

Breast cancer is 5th fatal cancer type which was accounted for 627000 deaths and quite common among women according to 2008 datas [1]. It also is supposed to need a bunch of stage to lead death like the others. These stages begin with abnormal growth of malignant cells and invasion of these around local tissue and proceed with metastasis process. After invade into extracellular matrix(ECM) of stromal layer, cancer cells enter blood flow defined as intravasation and circulate through bloodstream. Then they attach to blood vessel and migrate into another tissue/organ by penetrating blood vessel wall (extravasation). Finally, they localize and form tumor in distant tissue/organ and this termination called metastasis based on seed and soil hypothesis [2,3]. Herein, metastasis is really crucial point because it causes 90% death of cancer related diseases [3]. It has still unanswered questions and many factors involved in this process.

MDAMB231 is highly aggressive and metastatic breast cancer cell line. It classified as basal-like and tend to show mesenchymal transition [4] and really robust for drug treatments because of absence estrogen, progesterone and human epidermal growth factor receptor 2. That's why it is mostly called triple negative phenotype. Moreover, p53 and BRCA1 mutation which both are tumor suppressor factors in cells can mostly be seen in patients suffer from breast cancer [5]. On the other hand, MCF10A is normal human breast epithelial cells but it is triple negative, too [6]. Although it exhibits basal phenotypes, it can show luminal characteristic such as N-cadherin, vimentin etc. in turns out that it can tend to differentiate from epithelial characteristic to mesenchymal [5]. Nevertheless, its p53 is wild type in the contrary of MDAMB231 has mutated p53 [6].

1.2. Hypoxia, Physoxia and Normoxia

Oxygen amount is well known fact in terms of whole body management and this is pivotal for homeostasis. This amount can vary from cells and tissue to organ according to oxygen supply [7]. At this point there are a couple of terms define this situation. Firstly, normoxia describes atmospheric oxygen level which is 21% as known although this amount is not relevant physiologically. Next term called physoxia expresses physiological normoxia which is equal to 3-7% oxygen amount. Finally, hypoxia which its oxygen content is likely around 1-3% [8] and it can be mentioned when inadequate oxygen which thought below physiologic level supplied to tissue through blood in term of medicine [7]. Besides pathological hypoxia referred when oxygen amount is defined as 0.1-0.5% and generally found below 2% [8]. Aerobic metabolism got changed to anaerobic metabolism when considering hypoxia [9].

1.3. Energy Metabolism in Cells

As known, cells need energy for maintain their life and balance its metabolism. This energy generally called ATP and when it undergoes hydrolysis to ADP and AMP by taking 1 and 2 phosphates out respectively, cells gain its energy as free energy. They also produce this energy in the metabolic loop is essential for homeostasis by breaking down of organic molecules such as some amino acids, glycerol, nucleotides, carbohydrates especially glucose in the absence (anaerobic) and presence (aerobic) of oxygen. Firstly, as anaerobic metabolism glucose ($C_6H_{12}O_6$) is converted to pyruvate ($C_3H_4O_3$) and 2 ATP entirely is gained in this step mostly called glycolysis. Moreover, 2 molecules NADH (Nicotinamide adenine dinucleotide) produced and it will serve as electron supply for aerobic energy metabolism and activator in conversion of pyruvate to lactic acid and ethanol in terms of anaerobic metabolism. Next process facilitated in 3 steps regarding aerobic metabolism. First step is glycolysis just like anaerobic metabolism in cytosol of cell. 2nd step includes decarboxylation of pyruvate as CO_2 thus pyruvate with 2 carbons generate acetyl CoA by binding to CoA in mitochondria. As a result of this step 1 more molecule NADH produced per a pyruvate which is being utilized for further step. Final step is called citric acid or Krebs cycle and most of energy produced in

this step and occurs in mitochondria as well when compared to anaerobic metabolism [10]. During hypoxia, glycolysis is supported despite aerobic metabolism for the loss of oxygen. Even if adequate oxygen exists in environment, cells especially cancer cells sometimes prefer glycolytic pathway as if no oxygen exist. They amplify acidity of extracellular matrix by producing lactic acid. In doing so, they gain great opportunity for metastasis over the other cells because of aggressiveness [11].

1.4. HIF1α Mechanism and Simulation of Hypoxia

HIF is transcription factor that mediates several pathways against oxygen fluctuation especially in low oxygen. The most important members of this family are HIF1 and HIF2. One resembles another one and because of similar structure that includes similar sequence. Also both of them can be regulated according to oxygen level. Regarding HIF1, it consists of two subunits as α and β. Although HIF1β is constituted anytime for metabolism, HIF1α becomes active in low oxygen situation. When oxidative metabolism transitioned to low oxygen partially glycolysis, Prolyl hydroxylase tend to degrade/hydroxylate HIF1α but it can be resist in low oxygen case against this enzyme because of absence of oxygen which is utilized as substrate by prolyl hydroxylase. Besides, von Hippel-Lindau protein (pVHL) which is tumor suppressor protein binding to HIF1α is prevented so HIF1α degredation and ubiquination is interrupted thus it is directed to nucleus and localize over there. As a result, it links to Hypoxic responsive element which placed promoter region of hypoxia related genes and finally this specific genes transcripted. In the contrary case which is normoxia, HIF1α is being hydroxylated by prolyl hydroxlase as expected and pVHL binds to HIF1α as well [9,11,12,13,14]. This hydroxylation can be tightly interrupted without low oxygen requirement. Something like protease inhibitor, transition metals etc. can make it alone as if environment is fully hypoxic [13]. Cobalt which is transition metal is commonly used for this purpose by binding to iron part of prolyl hydroxylase so it inhibits both hydroxylation and degradation of HIF1 by prolyl hydroxylase and pVHL respectively. In doing so, HIF1α remains stabilized and accumulated in nucleus to initiate transcription of target genes [15].

1.5. HIF1 Related Genes Responsible for Metastasis

Oxygenation can be sharply reduced by poor blood flow and vascular deficit and it causes several pathways of diseases formation such as genetic instability, angiogenesis, apoptosis, invasion and metastasis of cancer cells [9]. Besides, distance of capillaries to tumor tissues affects oxygen transportation into tumor and it becomes more malignant type because of hypoxic situation [8]. This malignancy is conducted through several upregulated genes such as VEGF, IL8, CXCR etc. [8]. Angiopoietin-like-4 is highly associated with HIF1, too and plays an important role for impairing endothelial cells structure by affecting cell to cell junctions and inhibiting p53 transcription factor in terms of extravasation of breast cancer cells [8,11]. It expressed in endothelial cells during hypoxia, too [16]. Similarly, vascular endothelial growth factor (VEGF) breaks down endothelial barrier and ultimately increase vascular permeability by linking to its receptor VEGFR dependent with HIF1 in endothelial cells [11,12,17,18,19]. Moreover, VEGF induce angiogenesis from tumor during hypoxia [9,20]. Regarding endothelial cells, 6 hours hypoxic exposure induces shrinking of VE-Cadherin of endothelial cells so obviously this disrupts cell-cell junctions of endothelial cells [21]. To given an example, high level of VEGF observed in breast cancer and ultimately this disrupted brain microvascular endothelial cell structure during hypoxia [18]. HIF1 controlled secretory factors like osteopontin secreted by breast cancer cells when hypoxic requirements are met facilitates cell-matrix interaction especially in bone tissue [11]. When HIF1α activated in triple negative breast cancer cells somehow, they attached into luminal surface of blood vessel easily through L1CAM molecule which induced by HIF1 [17]. Lysly oxidase(LOX) also triggers invasion and metastasis through crosslinking into collagen I and IV and elastin as well as matrigel. This amine oxidase is likely reached to high level in hypoxia and prepare metastatic niche for cancer cells because of ECM remodeling [19,22]. Moreover, HIF1 mediate tumor growth and metastasis through several oncogenic pathways such as RAS, EGFR and tyrosine kinase receptor [9].

1.6. Biophysical Aspects of Hypoxia and Related Terms for Physiology

As mentioned above, both upregulated genes and vascular functions such as low perfusion, distance etc. play an important role in tumor progression. Moreover, oxygen consumption of abnormal grown tumor cells in tissue affects oxygen level of their need [19]. In terms of blood flow, acute, chronic and their subtypes give rise to transition to hypoxic state of tumor [8,23,24]. Acute hypoxia as the name suggests define short hypoxia term varies 20 minute to 2 hours. On the other hand, blood vessel feeding tumor tissue has low oxygen content which is corresponding to hypoxemic hypoxia because of clogging of vessel lumen with fibrin agglomerates, blood and tumor cells, innate low oxygen content and perhaps interrupted and poor blood flow [9,23]. Perfusion is limited in a way [8,23]. Like acute hypoxia, low oxygen and perfusion discrepancies from arteries to vein and capillaries can be seen in during chronic hypoxia. Additionally, it takes more than 2 hours in parallel with vessel distance to tumor and vascular remodeling [23]. Tumor regions where state both in normoxic and hypoxic may be shaped in terms of oxygen supplying to blood vessel in this case [19]. Last physiologic hypoxia which we are interested in called anemic hypoxia describes low Hemoglobin amount directly correlation with low oxygen amount just like hypoxemic hypoxia [25]. It can be seen in high altitude [20,26]. As subtype, functional anemia hypoxia can be included in this group that define smokers in which carbonmonoxide content can sharply ascending and finally declines oxygen amount. Anemic Hypoxia can be counted in both acute and chronic hypoxia but it is mostly in chronic model and it is utilized for theraphy based approach against tumor [23]. According to literature, acute hypoxia is tent to be more dangerous when compared to chronic hypoxia. Although tumor tries to survive in tissue during chronic hypoxia, it is willing to create new vessels so it can invade and subsequently disseminates through newly formed vessels as long as angiogenesis targeting chemotherapy and radio theraphy are conducted [8]. Once tumor cells undergo hypoxia, they maintain this phenotype even if they are in the normoxic state [17]. Moreover, it triggers reactive oxygen species by transition of glycolytic pathyway to TCA cycle because of being temporary situation [27]. Indeed, tumor is capable of live and become more malignant through proangiogenic factors against to hypoxia during chronic model. As mentioned above, therapies should be reshaped without the need

to base vascularization [8]. Novel therapies generally focused on increase blood flow which is tunable and oxygen delivery in the perfusion. In addition to these, Erythropoietin supplementation is likely stabilized the hypoxic situation and make chemotherapy efficient for tumor. Regarding hypoxia, proline hydroxylase and RAS targeted therapies should be improved [9].

1.7. Microfluidics and Lab-on-a chip Devices

Many studies have been conducted in vivo and in vitro to elucidate biological mechanisms. Studies in the field of cancer are also carried out mostly in vivo and in vitro. Although The studies carried out in vivo provide the possibility of physiological outcome because they can naturally build complex metastasis cascade, the applicability of imaging and reproducibility in terms of nonparametric data due to changes of conditions in experimental repeats is restricted. When compared to in vivo models for cancer research, in vitro models can serve highly controllable experiment and measurable parametric data. However, its use is limited by its inability to provide fully complete microenvironment and physiological relevance like in vivo systems. Nevertheless, in vitro studies are being developed day by day to reduce limitations especially in mimicking the physiological environment as proper as in vivo systems [28]. At this point, 3D in vitro systems developed unlike 2D in vitro systems. Among them, lab-on-a chips using microfluidic technology are widely used. Microfluidics enable small volume and energy consumption, high throughput because of small size and controllable 3D physiological relevant environment by using multidisciplinary fields such as physics, chemistry, biology etc. in lab-on-a chip. Although its performance needs to be improved in terms of demonstrating intercellular molecular and chemical communication, it allows for the real-time visualization of many cell-cell, cell-matrix interactions because of innate transparency [29].

1.8. Previous Literature Summary

As mentioned above extravasation is crucial step of metastasis and it is studied mostly. However, extravasation and hypoxia relation is still quite confusing

and controversial issue in the literature. Some paper found out significant increasing of extravasation during hypoxic exposure but others don't agree with them and suggest opposite results.

One of the study among protagonists showed that MDAMB231 extravasation towards lung increased with hypoxia according to both in vitro and in vivo assays [30]. Similarly, endothelial HIF1α deletion was shown to mitigate tumor cell migration through endothelial cells in vivo model [12]. A recent paper dealing with hypoxia, breast cancer and lab-on-a chip technology demonstrated more extravasation of breast cancer cells with hypoxia comparing to normoxia [31].

On the contrary of these papers, one paper investigating invasive potential of MDAMB231 and HT1080 by simulating extravasation under oxic and various low oxygen conditions stated that invasiveness of these cell lines have no significant behavior between oxic and hypoxic conditions [32]. Besides, in vivo study looking into effects of angiopoietin-like-4 protein activated in hypoxia on extravasation showed inhibitory effect of this protein on extravasation to lung [16]. Another study laid emphasis on decreasing of breast cancer cells extravasation through HUVEC with HIF1α insertion. However, they also showed angiogenesis of HUVEC with breast cancer cells [33].

1.9. Aim

In this study we investigated effect of HIF1α which is hypoxia indicator on breast cancer extravasation by comparing to normoxia/physoxia. This study represents both anemic-hypoxemic hypoxia physiologically and lead to understand underlying mechanism of extravasation into extracellular matrix related to low oxygen circulating through blood. In addition to HIF1α effects on that, dynamic perfusion flow was applied to determine effects on extravasation. Unlike previous literature, we try to understand and the effect of HIF1α activated endothelial structure in accordance with physiology by preconditioning them classified as severe and mild apart from circulated cells.

CHAPTER 2

MATERIALS AND METHODS

2.1. Device Fabrication

Device fabrication consists of photolithography and soft lithography steps. All steps related to photolithography gently and carefully performed in Applied Quantum Research Center Clean Room (Department of Physics, Izmir Institute of Technology) as previously notated [34]. SU-8 2075 Negative photoresist. Primarily SU-8 2075 (Micro Chem. Corp) epoxy based negative photoresist to be either dissolve in developer or not in the amount of 4-5 ml poured on silicon wafer substrate (University Wafer, Inc.) initially. Then, silicon substrate with SU-8 2075 negative photoresist rotated by means of spin coater (Specialty Coating Systems) in order to spread all around of substrate. Because of viscousness of photoresist, 1000 rpm with 50 ramp and 25 dwell operators in 3 steps were adjusted for obtaining thin and low height of channels. After that it placed on hot plate (Wise Stir MSH-20D) at 65^0C for 5 minute and then 95^0C for a hour to let resist attach to substrate. After all baking procedures completed, it held on a bench for overnight. Next day silicon wafer with SU-8 2075 photoresist placed on hot plate again 95^0C to control whether previous baking was enough or not. To clear wrinkle observation is possible with placing on bench dramatically after 95^0C. When it has been seen, it should be placed on 95^0C again. This procedure keeps going recurrently until no wrinkle is observed. Then silicon wafer with design previously drawn through Corel Draw software and printed on transparent mask in the 3600 dpi resolution (Figure 2.1) exposed UV light for 30 second through mask aligner (OAI Mask Aligner Hybralign Series 200). In this step, we should avoid to leave transparent side of mask on silicon wafer. For native chemical properties of negative photoresist, opaque side of design should be exposed to UV and unexposed parts finally will be dissolved. Crosslinking interaction between UV and photoresist requires thermal step one more time. Therefore, UV exposed silicon wafer placed on hot plate 65^0C for 5 minute and 95^0C for 10 minute respectively. After that it placed on bench for overnight. On following day, SU-8

Developer (Micro Chem. Corp) used for develop exposed areas. SU-8 developer applied without shaking in first 5 minute. After that, SU-8 developer gradually applied with shaking and checked out through stereo microscopy (Nikon Photonic PL2000). Besides, this process continued until no white precipitations were observed after 2-propanol (Emsure) applied. However, this process is never enough alone so stereo microscopy should be used to see all clear developing. Nevertheless, 2-propanol test usually shows former steps verification. Soft lithography has been just begun anymore.

Master mold (Figure 2.2) was brought over from clean room was introduced with polydimethylsiloxane (Sylgard 184, Dow Chemical). Polydimethysiloxane, PDMS is polymer and consists of silicon elastomer and curing agent. Firstly, silicon elastomer and curing agent was prepared 10:1 ratio and mixed. Degassing was applied to mixture in vacuum chamber to avoid air. Mixture was separated from bubbles poured into master mold contains device design and it was kept in room temperature until it is polymerized on which it takes approximately 2 days. After polymerized PDMS (Figure 2.3) was cleaned with several procedures such as ultrapure H20, 70% Ethyl alcohol (Emsure) and ultrasonication, flow channel was punched 2mm and the rest of channels were punched 1.5mm puncher to fit 100-1000 ul pipetor tip. After cleaning process, it was dried and sealed into glass irreversibly through UV/Ozone plasma (Bioforce Nanosciences) In this procedure, hydrophilic PDMS become hydrophobic by crosslinking with oxygen. Then it was placed on hot plate at 100^0C for 10min in order to be sticker. Sealed PDMS was treated with UV light at 15 minute for sterilization. Finally, it will be ready to observations or further experiments.

Our design consists of 3 channel separated from each other with pentagonal posts. Channels were named flow, matrix and reservoir channel respectively. Matrix channel length and width are 1cm and 1mm respectively for handling. There are 5 gap between 6 post separate matrix and flow channel. Each gap was designed in the size of 200 μm equally. Flow channel dimension is 1mm width x 15mm length. However, the height of this channel is photolithography dependent because of manuel handling. It varies broad range of amount. Yet, this trait should be known and accounted for shear stress calculation and endothelial monolayer formation.

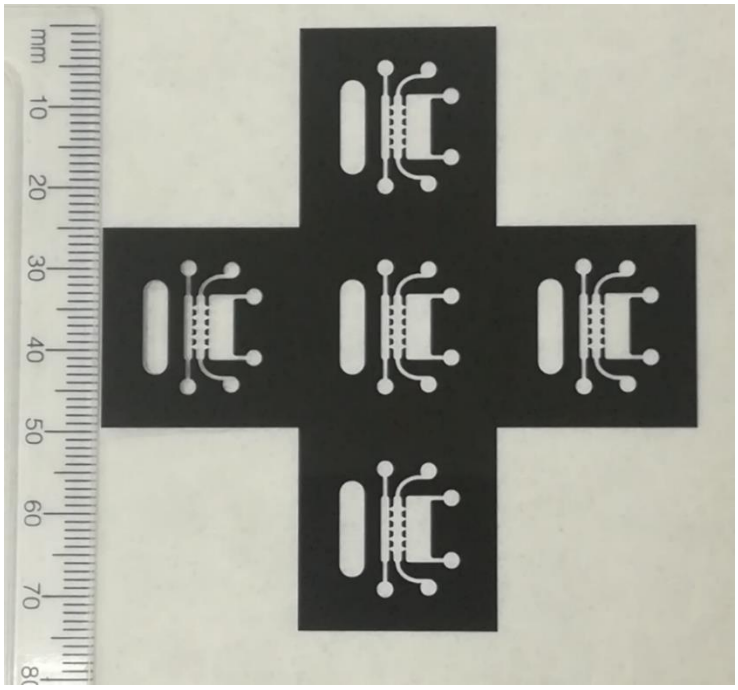

Figure 2.1. The Pattern to be printed on the master mold with UV lithography.

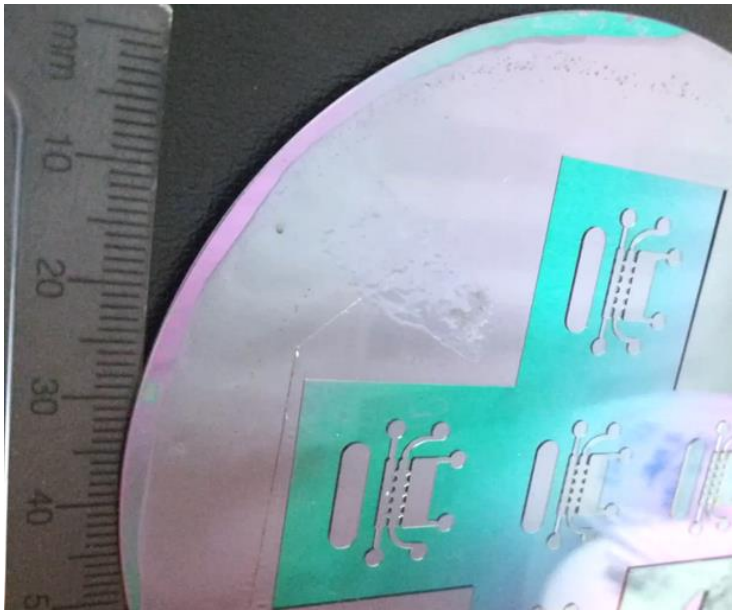

Figure 2.2. The master mold prepared with UV lithography.

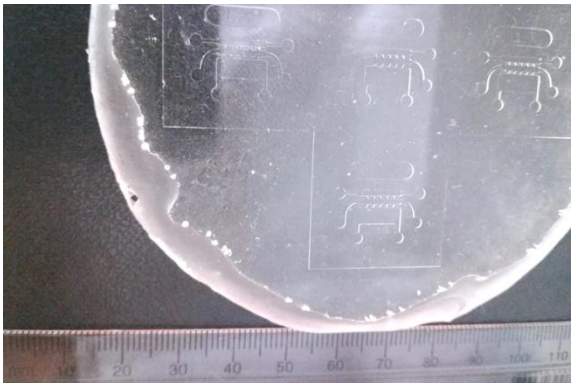

Figure 2.3. The state of the polymerized PDMS as a result of soft lithography after removal from master mold.

In order to know the height of flow channel, a piece was cut out from flow channel side. A photo of this section was taken under light microscopy with 5x objective. Standart rulers all dimensions known and calibrated were snapped simultenously. First, straight line was drawn between start point of line and end point of the other line by using IMAGEJ (Fiji). Length of drawn line shown top circle (Figure 2.4) in the pixel unit was measured with ctrl+M shortcut. This length is equal to 200 µm. One more straight line was drawn again within bottom circle (Figure 2.4). It was measured with same shortcut and calculated by considering its length according to rulers proportionally.

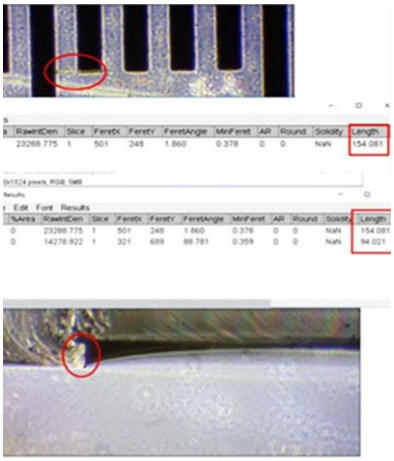

Figure 2.4. A photo showing how to measure height of channel.

2.2. Device Coating

Lab-on-a chip devices were coated to assist endothelial cells and matrix attachment. To better understand which protein is most efficient for attachment, various protein strategy was conducted. Poli-L-Lysine, PLL (0.01 mg/ml, P2682, Sigma-Aldrich) was introduced with channels as a first strategy.I It held at 37^0C for overnight and taken out from device and washed with ultrapure water for 3 times in following day. After that it was allowed to hold at 80^0C for 24 hour in order to gain hydrophobicity again and Fibronectin (0.0125 mg/ml, Sigma, F2006) was loaded into channel then placed in 37^0C with 5% CO_2 incubator for an hour. Finally it washed with 1x Universal Buffer and Autoclaved ultrapure water 3 times for each and placed vacuum dessicator to save protein against thermal degradation. Another approach is that Channels coated with 2% 3-aminopropyltriethoxysilane, APTES (Sigma Aldrich, A3648) in acetone for 15 minute at room temperature [35]. Then, they washed with 1x PBS and Autoclaved ultrapure water 3 times for each. Subsequently, Laminin (0.0125 mg/ml, Sigma, L2020) was loaded into channels and placed in 37^0C incubator with 5% CO_2 for 1 hour. Finally, they washed with 1x Universal Buffer and Autoclaved ultrapure water 3 times for each. After their wet removed through vacuum suction, they placed in vacuum chamber overnight prior to use in experiments. As 3rd strategy, Fibronectin was conducted in the same way with laminin after APTES loading. Collagen type I (354236, Corning) dissolved in DMEM High Glucose Medium (O1-055-1A,Biological Industries) without any serum in the dilution of 0.0125 mg/ml. After APTES loading and washing, it was loaded into channel and allowed to hold at 37^0C for 1hour. Then it washed with serum free DMEM High Glucose Medium and Autoclaved ultrapure water 3 times for each.

2.3. Cell Lines Preparation and Tracking

MDAMB231 invasive breast cancer cell line purchased from (ATCC). It cultured in tissue cultured petri dish with DMEM High Glucose (01-055-1A, Biological Industries) media supplemented with %10 FBS (04-001-1A, Biological Industries), %1 Penicillium-Streptomycine (03-031-1B,Biological Industries), %1 L-Glutamine(03-020-1B,Biological Industries) at 370C incubator with 5% CO2. Cells were not splited more than passage 45. bEnd.3 mouse brain endothelial cell

line was obtained from (ATCC). In this study, bEnd.3 mostly were in the charge of endothelial monolayer formation instead of HUVEC (Human umbilical vein endothelial cell). However, there is no significant effects on extravasation between HUVEC and bEnd.3 as indicated in previously published paper [36]. It also cultured in tissue cultured petri dish with DMEM High Glucose media as same as MDAMB231 cell line at 37^0C with 5% CO2. These cells below passage 40 were used in all experiments. MCF10A normal breast epithelial cell lines commercially supplied from(ATCC). It cultured in tissue cultured petri dish with DMEM F12-HAM (01-170-1A, Biological Industries) solution supplemented with 5% Donor Horse Serum (04-004-1A, Biological Industries), 20 ng/ml EGF (E9644, Sigma), 0.5 µg/ml Hydrocortisone (H0888, Sigma), 100 ng/ml Choleratoxin (C8052, Sigma), 10 µg/ml Insulin (I1882, Sigma), 1% penicillin/streptomycin (03-031-1B, Biological Industries), 1% L-glutamine (03-020-1B, Biological Industries) at 37^0C with 5%CO2. They were used in the range of passage 5-30. All of them are trypsinized and collected from sub-culturing. While bEnd.3 cells stained with 5 µm Green CMFDA cell tracker (Invitrogen), MDAMB231 and MCF10A cells stained with 10 µm Red Tracker CMTPX (Invitrogen, C34552). They observed under fluorescence microscopy (ZEISS HAL 100) if they stained with dyes. All cells counted to obtain desired numbers by means of EVE Automatic Cell counter (NanoEntek).

2.4. Cell Loading and Gel Preparation

For initial step of experiments, growth factor reduced Matrigel (Corning, 356230) was diluted to 4 mg/ml with DMEM high Glucose Medium and loaded into matrix channel for 35 minute. In doing so, nutrient independent extravasation was aimed by using growth factor reduced matrigel. Then reservoir channels filled with complete medium and endothelial cells at appropriate number were loaded into flow channel. Endothelial cell number can be varied height to height. It forms a basis of 2^{nd} optimization step of endothelial monolayer dependent with coating optimization. Endothelial cells suspended in 8% 450-650 kDa dextran (31392, Sigma) after centrifugation according to previously described [37]. (Figure A.4, Figure A.5) After loading cells, they placed on staining jar with autoclaved ultrapure water towards posts overnight as shown (Figure 2.5) according to previously described [38].

Endothelial monolayer formation was observed under confocal microscopy (Leica, DMI8) with 10x objective in and 1% 488 laser at each posts with 15.04 µm z interval throughout height of channel. While the intact monolayer structure at posts was considered and prepared for extravasation event, nonintact structures were omitted (Figure 2.8).

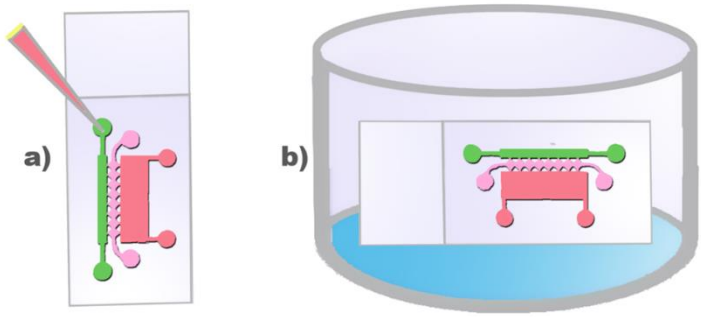

Figure 2.5. An image representing loading and settling of endothelial cells for endothelial monolayer formation. a)loading of cells b)settling down of lab-on-a chip with cells in staining jar overnight.

2.5. Flow Optimization

To better mimicking perfusion through blood vessel without any damage against blood vessel-like structure, gravity driven flow was applied on the basis of height difference. Flow rate to height difference adopted to our rotator (Multi BioRad RS-24, BioSan) based on previous study [39]. First 5, 10, 15, 20 degree angles were applied in 1 rpm and snapped at start and finish time of center of inlet and outlet gaps according to angle to determine how well it transpositioned in terms of height against degree (Figure 2.6). Then these values processed in IMAGEJ to define actual height difference between both gaps by accepting ruler as a measure. Then following formula from former paper [41] defined as Pouseille Flow in rectangular shape which is equal to our system.

$$Q \approx \frac{h^3 w \Delta p}{12 \eta L}\left[1 - 0.630\frac{h}{w}\right], \text{ for h} < \text{w}$$

"Q" is volumetric flow rate in the m3/sec unit, "h" is height of channel as a meter and "w" is width of channel as a meter as well, "Δp" defines pressure difference in the Pa unit , "η" is corresponding to viscosity in the Pa*sec and "L" is

length throughout channel as a meter. This formula is relevant for our system because height of channel is smaller than width of channel. Δp can be expanded with density (ρ,kg/m3), gravity coefficient (g, m/sec2) and height difference between inlet and outlet (Δh, m). Thus, following formula can be obtained.

$$Q \approx \frac{h^3 w \rho g \Delta h}{12 \eta L}\left[1 - 0.630\frac{h}{w}\right], \text{ for h} < \text{w}$$

So far, all values were measurable and known. However, wall shear stress should be known for maintaining endothelial monolayer well structure. Thus, volumetric flow rate can be integrated as flow rate as ml/min into following formula to know shear stress to be applied corresponding to height difference between inlet and outlet [35].

$$\tau = \frac{6\eta Q}{wh^2}$$

"τ" is equal to shear stress in the Pa unit, "Q" is actual flow rate in the ml/min unit, "η" is corresponding to viscosity in the Pa*sec, "h" is height of channel as a meter and "w" is width of channel as a meter. Calculated shear stress gave angle to be applied in rotator because of combination of equations by converting height of difference angle to radius unit by means of table.(Figure A.6)

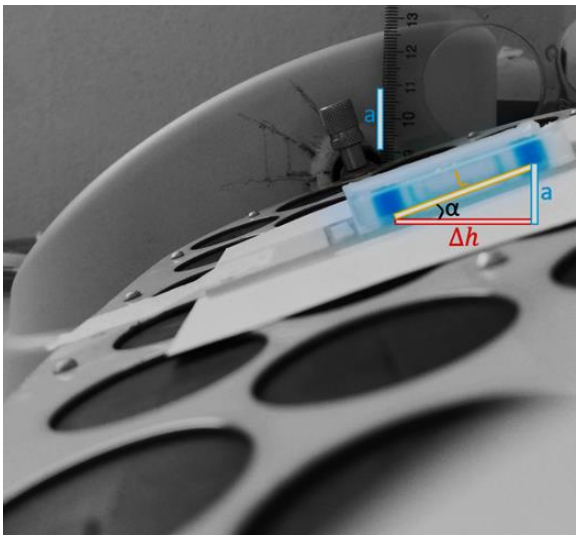

Figure 2.6. An image showing the height difference and length at the inlet and outlet according to angle set at the rotator for flow optimization.

All flow experiments set up to be 0.77 dyne/cm^2 which adjusted to be similar with vein shear stress in the range of 1-6 dyne/cm^2 [23,41] for 12 hours and continued

settle in dish without any flow until 24 hours are full. Static conditions maintained without any flow by settling in dish for 24 hours. To better quantification and observing extravasation, cell number of MDAMB231 and MCF10A to be circulated in flow channel are decided to be 50000 cells/ml because less number minimize extravasation efficiency while more number is hard to count according to paper previously stated [42,43]. Extravasation expected within 24 hours as literature stated before [44]

2.5. Endothelial Monolayer Integrity Assay

For endothelial monolayer integrity and investigating vascular geometry during hypoxia, 70 kDa fluorescently labelled dextran which is equal to albumin that is known it is confined in blood vessel was used in flow and static conditions from flow channel [45]. For this purpose 70 kDa TMR dextran (D1819, Life Sciences) was prepared in the ratio of 1:250 in 1x PBS. It was loaded into flow channel after endothelial monolayer formation and all positions including both flow channel and matrix channel was adjusted and their photo were taken by means of ZEISS Microscopy with 4x objective and 1500 ms exposure time of both 488 and 555 fluorescence in 1 and 30 minutes under static and dynamic cases. Then ROI in the dimension of 64.28 μm width x 28.57 μm height placed in certain places by using IMAGEJ (Figure 2.7). Mean intensity in gel region(ROI 1) of all conditions that are static normoxia, static hypoxia, static without endothelial barrier, flow normoxia, flow hypoxia and flow without endothelial barrier subtracted from background intensity (ROI 4) in 1 and 30 minutes and analyzed.

2.6. Cell Viability Assay

MCF10A, MDAMB231 and bEnd.3 cell viabilities against cobalt chloride was examined. They all were dissolved in DMEM High Glucose media supplemented with 10% FBS, %1 Penicillium-Streptomycine, %1 L-Glutamine and seeded into 24 well plate at 25000 cells/500ul(well) . After that, they were incubated in 37^0C incubator with 5% CO_2 overnight. Cobalt Chloride Hexahydrate, $CoCl_2$ (C8661, Sigma Aldrich) is utilized for hypoxic treatments. It was weighed and solubilized with

complete medium in appropriate concentrations. It was prepared in 100 µM final concentration.

All wells were labeled dead (70%EtOH), no $CoCl_2$ (Culture Media), 50 µM $CoCl_2$, 100 µm $CoCl_2$ respectively for each cell lines. Before $CoCl_2$ treatment, old medias removed for each and refreshed with new media only for 0 µM. After CoCl2 treatment at 50 and 100 µm doses, they placed in 37^0C incubator with 5% CO_2 for 24 hours. After 24 hours, 70% EtOH added into dead control well for 15 minute and Propidium Iodide (1:500, P4170, Sigma Aldrich) and bis-Benzimide H33342 trihydrochloride, Hoechst 33342 (1:50, B2261, Sigma Aldrich) dyes were added into each wells for 15 minute in 37^0C incubator with 5% CO_2 overnight. Then, 24 well plate placed upon Zeiss Microscope and photos were taken with 5x objective and phase contrast, 555 and 405 nm excitation length in 3 different positions per well. Photos were transferred to IMAGEJ software and Hoescht photos opened separately. All steps of Propidium Iodide are same as Hoechst 33342 photos and their image processes were conducted through as following steps.

Firstly "process>filters>gaussian blur" steps are followed respectively.10.00 radius value were generally applied in photo and it saved as different name for example "cellname_dose_hoe or p1_gb". Raw and blurred photos were opened again and process>image calculator tool was clicked. Then raw photo was selected as "Image 1" and blurred photo was selected "Image 2". Substract option was activated as operation module and OK clicked. New photo was ready to make threshold. "Image>adjust>threshold" steps were followed respectively. Threshold was arranged until any noise seen in photo. However, Same threshold value applied into propidium iodide photo. Then "process>binary>erode>dilate>watershed" steps applied separately and respectively for the purpose of remove noises and separate clustered cells. Subsequently "process>filters>variance" was activated and radius was adjusted 1 pixel. After that "process>binary>fill holes>watershed" was coming one more time separately and respectively. Finally, particles were counted by following "analyze>analyze particles". Counted numbers were saved as Hoescht position. Same steps applied for propidium iodide which equal position for Hoescht. After counted, propidium iodide numbers were saved and divided into related Hoescht position. It gives dead cells% in total cells. Finally, it was arranged viable cells% by substracting those from 100.

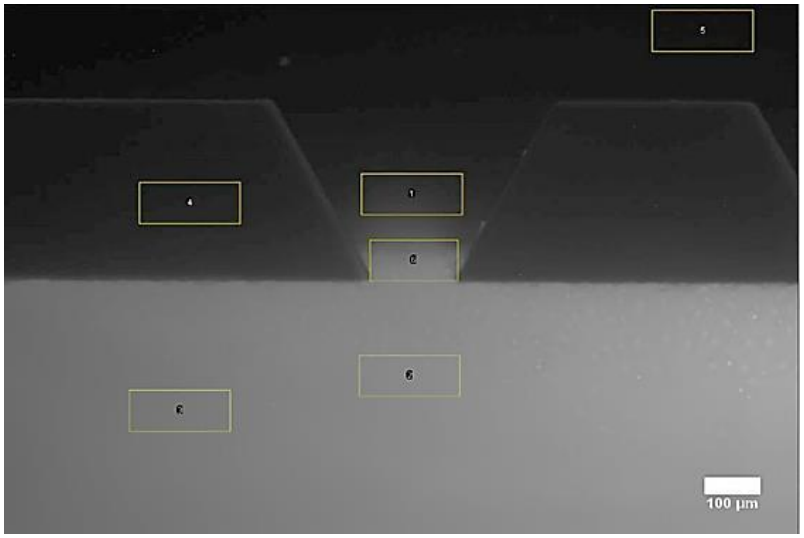

Figure 2.7. Image represents selected ROIs for endothelial monolayer integrity analysis. ROI-1 shows mean intensity in the gel region, ROI-4 is background intensity. Scale Bar:100 um

2.7. Determination of HIF1α Localization

For clear HIF1α observation, 50000 bEnd.3 cells/ml in 48 well were treated with 100 µM $CoCl_2$ for 4, 6, 8, 24 hours and only media without $CoCl_2$ (control) based on the study [46]. In this study bEnd3 cell lines preconditioned with $CoCl_2$ because hypoxia simulation only measured in nuclei of bEnd.3 cells. However, other cell lines show HIF1α localization in their nuclei as well (Figure A.2). Then all samples washed with 1x PBS and fixed with 4% PFA (15710, Electron Microscopy Sciences) in 1x PBS overnight. Then 0.1%Triton (T8787, Sigma) in 1X PBS applied to permeabilize for 15 minute. After washing with 1x PBS in 3 three times, they blocked with 1% Bovine Serum Albumin (A2153, Sigma) for 1 hour at room temperature. Subsequently Primary HIF1a antibody (sc13515, Santa Cruz) was introduced with cells at a dilution of 1:200 overnight. Secondary goat anti mouse antibody (A21127, Thermo Fischer) was replaced with primary antibody at a dilution of 1:400 for 1 hour at room temperature. Besides, cell nuclei were stained with DAPI at a dilution of 1:100 for 1 hour at room temperature. Finally they were mounted and screened through (OLYMPUS IX83) with 405 and 555 nm excitation length in 10x and 100x objective.

After data obtained, all images with DAPI proceed into Gaussian blur with 10.00 strength. Then, Original DAPI images subtracted from Gaussian filtered one(s)

through image calculator. After that, it adjusted to appropriate threshold. Subsequently, “process>binary>erode>dilate>fill holes>watershed” applied respectively and separately. Now, particles were ready for analysis. To analyze particle is really crucial step for one step beyond so ROI window should be avoided to close and it must be saved. For HIF1α photos, their background measured and they had no intensity background so they were ready for thresholding. However, if they had any mean value background when they checked, they must be subtracted through “process>math>subtract” respectively. Their threshold images obtained and ROI previously obtained applied HIF1α thresholded photos by clicking show all and labels. Then all ROIs were ready for measure. Both qualitative and quantitative analysis were performed.

For qualitative analysis, HIF1α positive nucleis were calculated following formula:

“ 100-(number of “0” or “NaN” mean values/ total particle)*100 ”

For quantitative analysis, All mean values in nuclei were only collected in a column for every condition separately.

2.8. Extravasated Cell Quantification and Extravasation Metric

After loading MDA-MB-231 and MCF10A into flow channel for 24 hours in flow and static condition, ROIs which defined according to intact monolayer at each post space was considered and investigated under LEICA Confocal Microscopy with 10x objective 1% 488 and 2% 555 lasers and 15.04 μm z interval throughout height of channel. Surface of posts with endothelial cells in the nonadjacent to gel region and Other side of channel without post were not taken into account for extravasation quantification. The photo frame was set by taking 360 μm from flow channel and 800 μm from matrix channel. Besides, it was accommodated midpoint of width for each post which is corresponding to 500 μm. For extravasation event, all ROI from selected posts divided into intact and nonintact monolayer in order to observe vascular damage caused by hypoxia (Figure 2.8).Then extravasated particles (Figure 2.9) which both must exit from endothelial monolayer structure and become nonvisible in this structure (Figure 2.10) and associated particles which are connected with the endothelial monolayer at the border of matrix and endothelial

monolayer and they are about to extravasate were counted by looking in 3D and 2D (Figure 2.11). Since fluorescence of the cells sometimes can be reduced, looking into cells in 2D with brightfield and 555 merged channel facilitates analysis (Figure 2.12). Moreover, all remaining cells in the endothelial monolayer structure were counted.

Regarding extravasation metric, it calculated with extravasated cells divided by posts. This helps to compensate post-based extravasation and complementary for particle quantification.

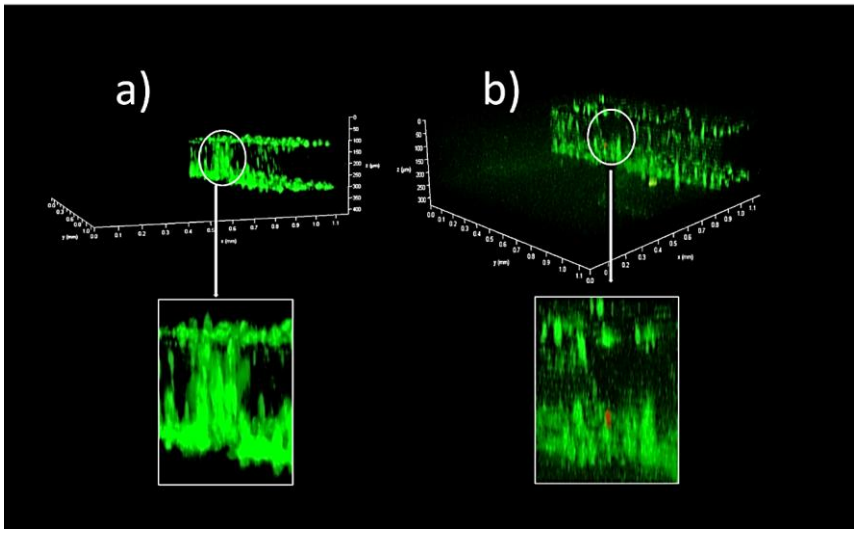

Figure 2.8. Representative image indicating a) intact b) nonintact monolayer

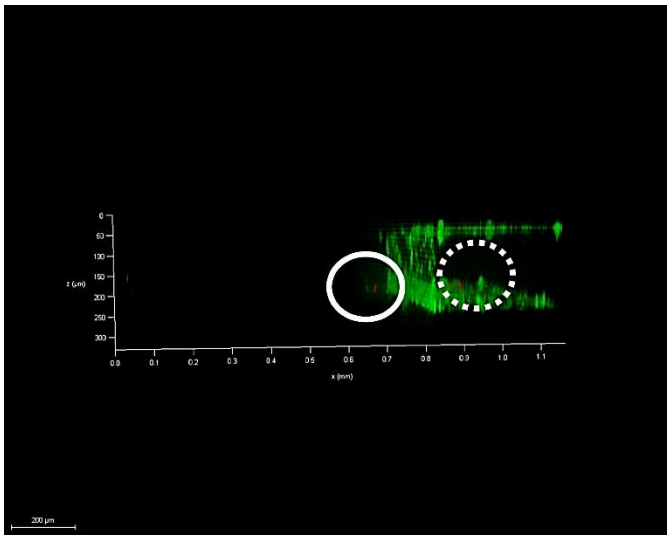

Figure 2.9. Representing image of extravasation. dashed circle: circulated cells in endothelial monolayer , straight circle: extravasated cells from endothelial monolayer. *=matrix, **=flow channel. Scale Bar: 200 μm.

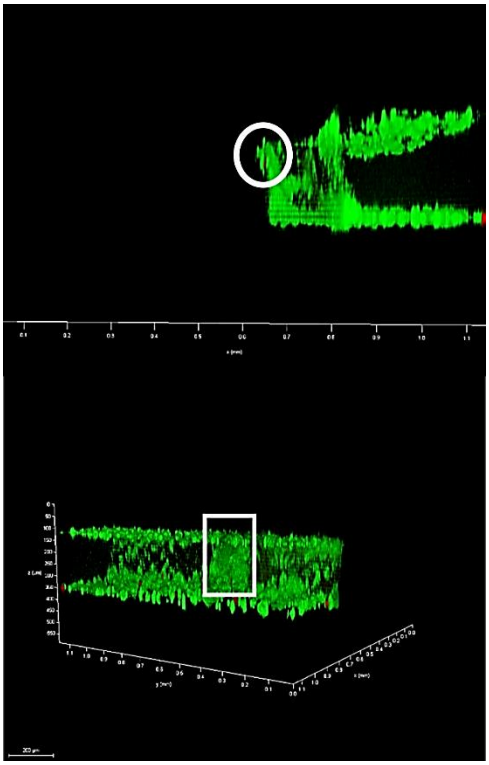

Figure 2.10. The appearance of the extravasated cell outside (top) the endothelial monolayer and invisibleness (bottom) inside the endothelial monolayer. green:endothelial cells, red: circulated cells. *=matrix,**=flow channel. Scale Bar: 200 μm.

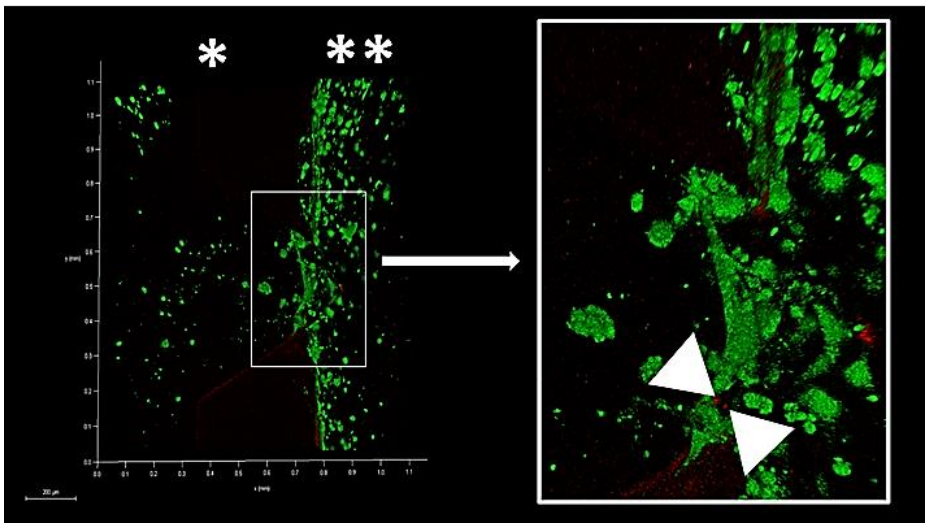

Figure 2.11. Representing image of associated cells adjacent to endothelial monolayer boundry between monolayer and matrix. green: endothelial cells, red: circulated cells. *=matrix,**=flow channel. (endothelial cells sometimes can migrate to matrix). Scale Bar: 200 μm.

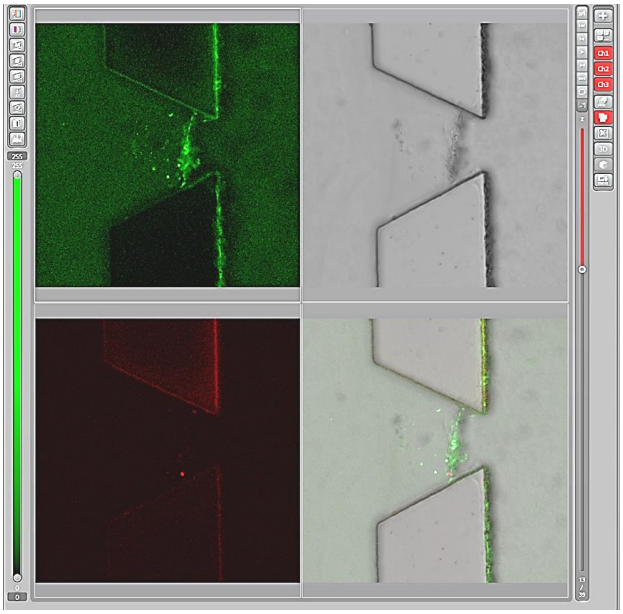

Figure 2.12. An image showing the brightfield, 488 and 555 fluorescence and merged channels for extravasation analysis in 2D.

2.9. Distance of Extravasated Cell Quantification

In addition to number of extravasated cells, distance of extravasation of each particle quantitatively measured. First extravasated ROIs opened in 2D with merged channel includes brightfield, 488 and 555 fluorescence channel. Z position of photo adjusted until particle is visible. At this point straight line was drawn throughout outermost point of endothelial monolayer in “y” position and other straight line was drawn from center of particle to outermost point of endothelial monolayer. This was repeated for each particle and collected. (Figure 2.13)

2.10. Statistical Analysis

All samples consist of at least 2 technical and 3 biological repeats. One way ANOVA followed by Tukey comparison was performed in cell viability assay and HIF1α localization. Extravasation Metric was conducted through Proportion test. Mann Whitney U non parametric test was applied in extravasation particle and distance analysis by means of GRAPHPAD Prism 5.0. Statistical significance was based on 0.05, 0.01 and 0.01 level when considering cell viability, HIF1α immunofluorescence, permeability and extravasation assays.

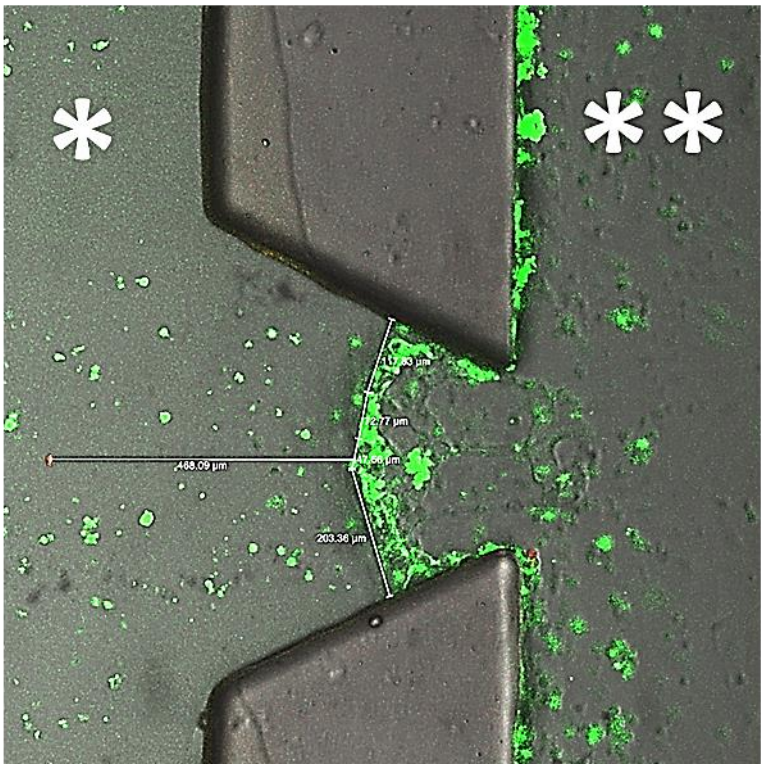

Figure 2.13. A photo showing the distance of the extravasated cell to the endothelial monolayer, which determines the outermost point of the endothelial monolayer and is extravasated in the same "Z" position. green: endothelial monolayer, red: extravasated cell. *=matrix, **=flow channel (endothelial cell sometimes can migrate to matrix channel)

CHAPTER 3

RESULTS

3.1. Effect of Cobalt Chloride on Cell Viabilities

To better understand effect of cobalt chloride which is hypoxia mimicking agent, MDAMB231, MCF10A and bEnd.3 cells to be utilized for extravasation experiments treated with $CoCl_2$ at different doses in 24 hours equal to time for extravasated cell observation.

After 24 hours, all cell viabilities significantly decreased considering 100 µm $CoCl_2$ when compared to normoxic (control) group. 100 µm $CoCl_2$ treated MDAMB231 showed more reaction than other cell types when compared to control (Figure 3.1). However, they were not significant from each other at each condition (Figure 3.2). That's why 100 µm $CoCl_2$ was selected for hypoxic simulating dose. Besides, other cell lines have never been seem to detached from petri dish when they pretreated with $CoCl_2$ show no viability when they seeded into non-treated petri dish to eliminate attachment (Figure A.1). Accuracy of our model was measured according to 70% EtOH samples. It is working with 96.74735±2.501573% precisely (Figure 3.3)

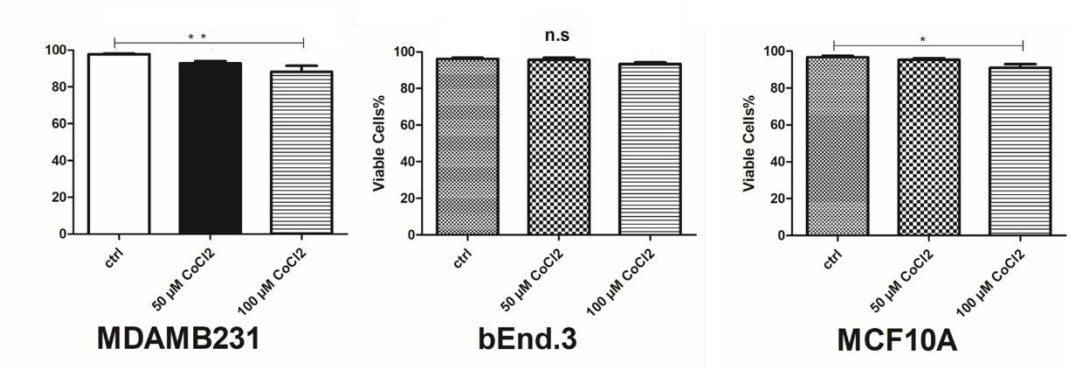

Figure 3.1. Effects of $CoCl_2$ on cell viabilities separately. *= p<0.05, **= p<0.01

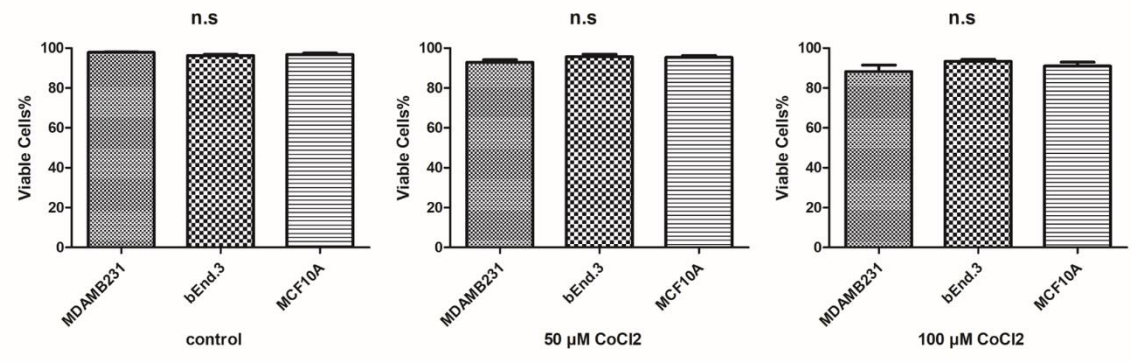

Figure 3.2. Effects of $CoCl_2$ among each other. n.s=not significant

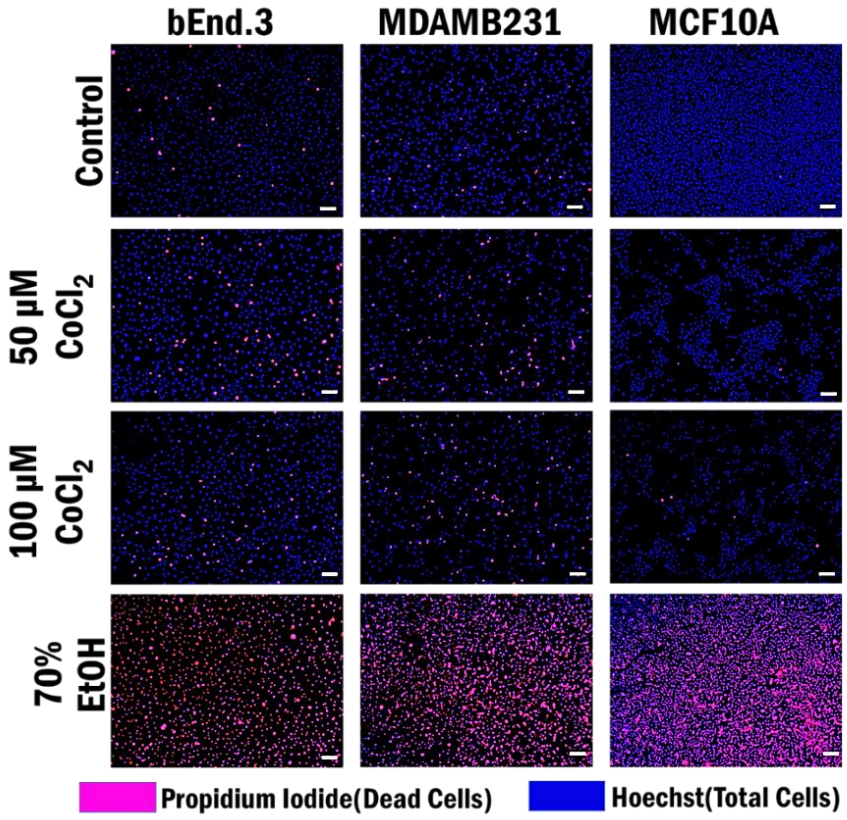

Figure 3.3. Different doses of $CoCl_2$ on bEnd.3, MDAMB231, MCF10A viabilities for 24 hours Scale Bar: 100 µm.

3.2. Determination of HIF1α Localization

To define how many times required for maximum HIF1α localization in nuclei of bEnd.3 cells, they exposed 100µm $CoCl_2$ at certain intervals. In our

procedure, HIF1α expression of bEnd.3 cells analyzed at certain interval because they have just pretreated with 100µm $CoCl_2$ apart from other cell types before extravasation experiments. During extravasation experiment for 24 hours all cell types show HIF1α localization in nucleus according to immunostaining. (Figure 3.4)

In terms of mean intensity all conditions are significantly different from each other. ($p<0.001$, Figure 3.5) It shows the HIF1α induction in nuclei with 100 µM $CoCl_2$ is time dependent issue. For sure, qualitative analysis was conducted whether HIF1α locate in nuclei or not. It shows 4 hours condition is significantly higher from each conditions($p<0.001$). In addition to these, 6 hours induction is different from 8 hour induction($p>0.05$) and significantly different from 24 hour and control samples. ($p<0.001$). Last but not least, 24 hour and control samples are not different from each other in terms of qualitative analysis. (Figure 3.6) Besides, 100x fluorescence photos confirm that qualitative and quantitative assays are complementary for each other. (Figure 3.7, Figure 3.8) That's why, similar differences between qualitative and quantitative analysis were taken into account in order to determine mild and severe hypoxic condition. Obviously, 4 hour and 6 hour 100µm $CoCl_2$ treatment were applied as severe and mild hypoxia mimicking case, respectively. Besides, 100µm $CoCl_2$ treatment reshapes the cellular morphology (Figure A.7).

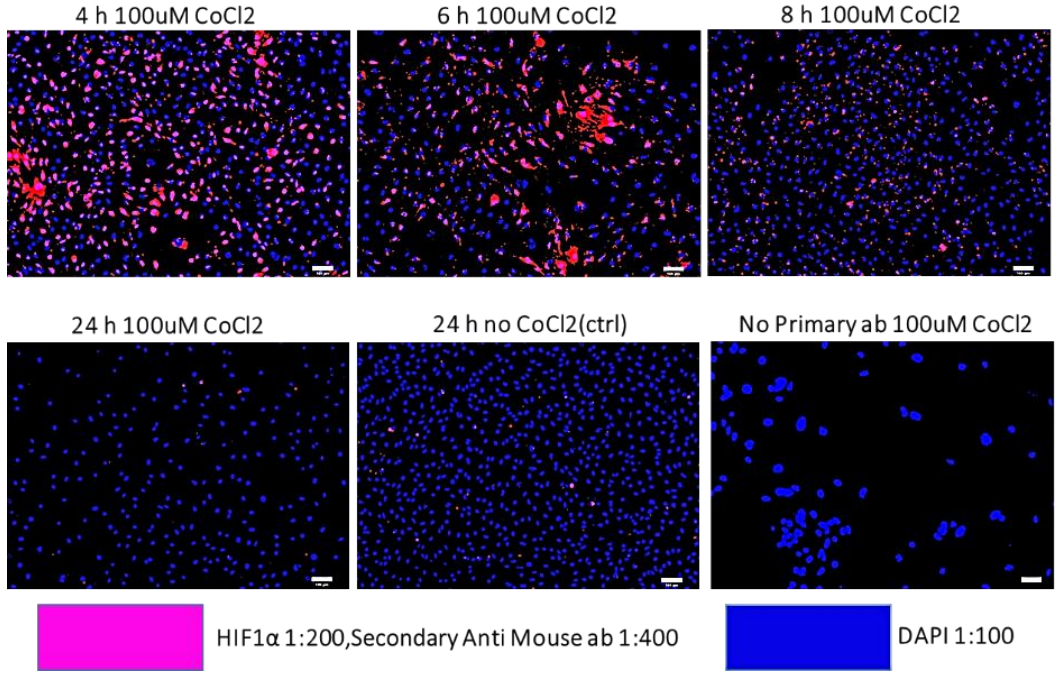

Figure 3.4. Image representing HIF1α localization in bEnd.3 nuclei at different time points. Scale Bar: 100 µm

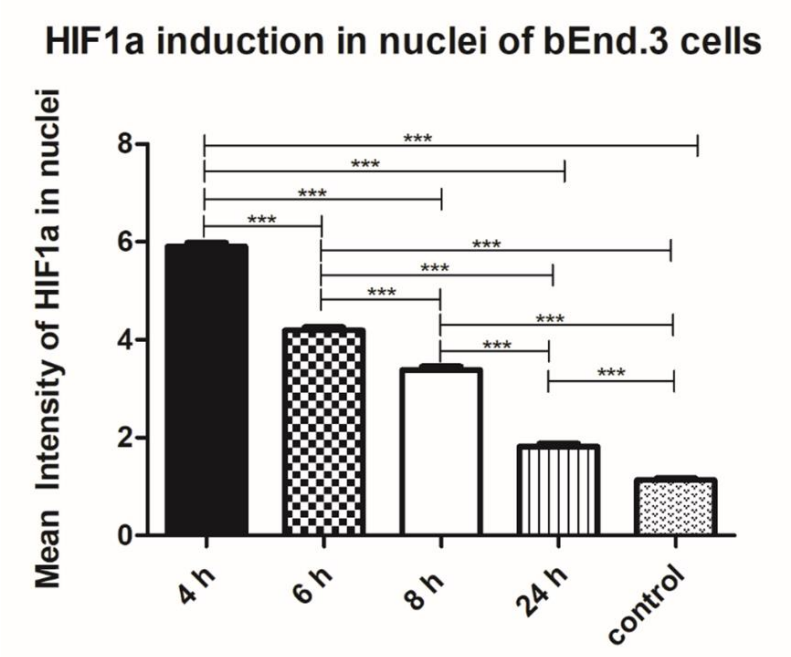

Figure 3.5. HIF1α localization in bEnd.3 nuclei at different time intervals with 100 μM $CoCl_2$ and without $CoCl_2$ (control) in terms of mean intensity of nuclei. ***= p<0.001

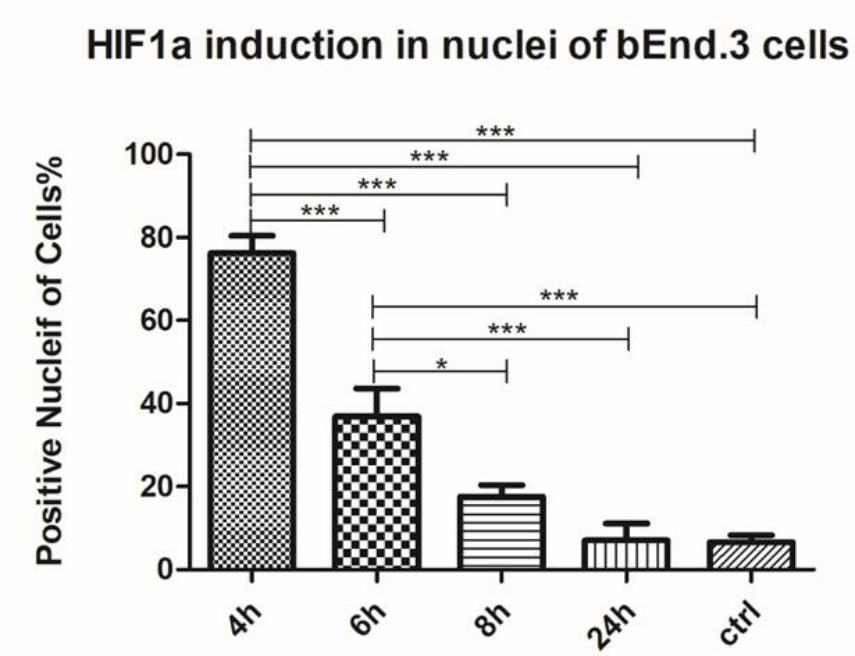

Figure 3.6. HIF1α localization in bEnd.3 nuclei at different time intervals with 100 μM $CoCl_2$ and without $CoCl_2$ (control) by searching any intensity in nuclei. *= p<0.05, ***= p<0.001

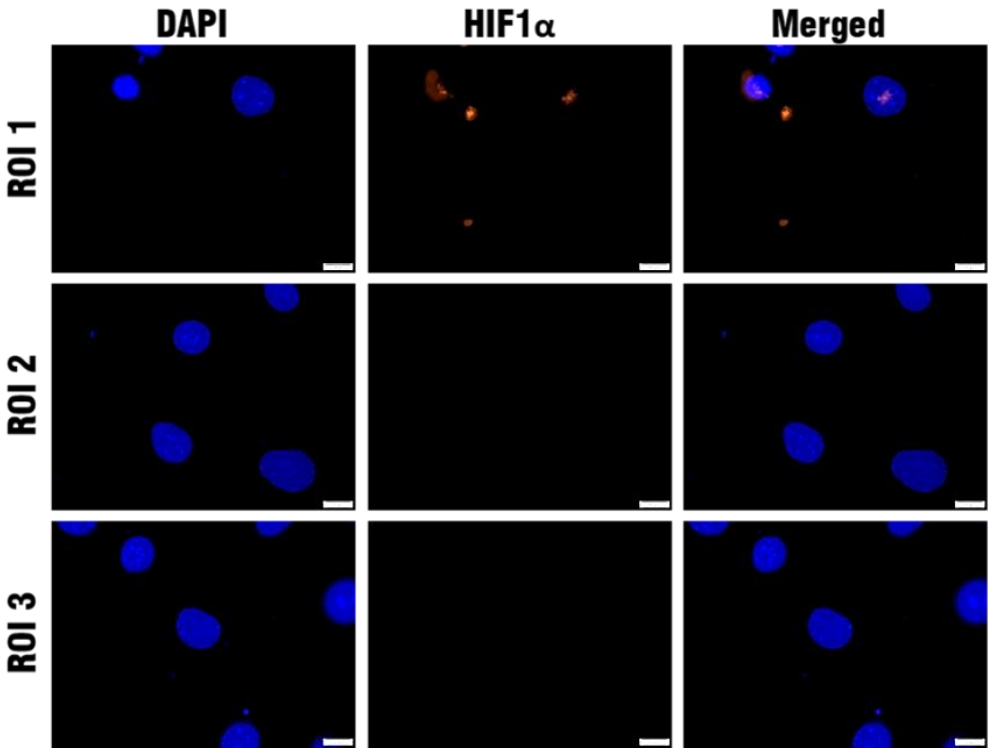

Figure 3.7. HIF1α localization in bEnd.3 cells nuclei without $CoCl_2$ in 100x objective. Scale Bar: 100 µm.

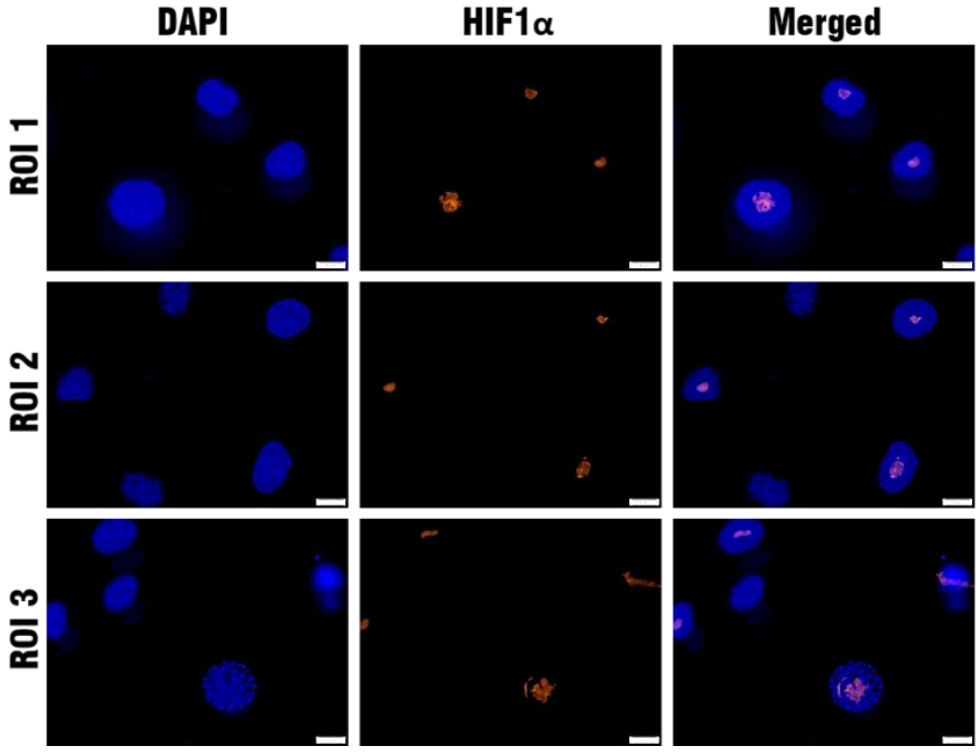

Figure 3.8. HIF1α localization in bEnd.3 cells nuclei with 100 µM $CoCl_2$ in 100x objective. Scale Bar: 100 µm

3.3. Effects of Coating and Cell Number on Endothelial Monolayer Formation

According to previous study [38], they manually handled in prospective intervals and it needs cell refreshment into channel. Unlike this study, once introducing of endothelial cells, it settled down and hung to reservoir channel overnight prior to observation in our model.

In terms of device coating, firstly poly-L-lysine (PLL) and APTES-fibronectin were compared. Although they showed similar performance in terms of endothelial monolayer formation, APTES-Fibronectin was firstly selected for further process. Since, the PLL coating takes more time than the APTES coating (Figure 3.9, Figure 3.10) After first selection of coating optimization, APTES-Laminin combination was preferred to further experiments. Other proteins such as collagen and fibronectin prepared at the same concentration as laminin were not as effective as laminin. (Figure 3.11) Collagen sometimes cause distorting of endothelial monolayer formation between flow and matrix channel and loading and handling of collagen can be trouble in the preparation of experiment. The contribution of fibronectin to endothelial monolayer formation is close to the laminin as same as collagen. In conclucion, APTES-laminin was utilized for all the experiments apart from collagen and fibronectin.

Regarding cell number, it was examined starting with 110000 cells/ml . Apparently, it was not enough to form endothelial monolayer. (Figure 3.12) That's why multiple cell numbers followed by 1500000 cells/ml. (Figure 3.12) This was quite promising because it was about to form endothelial monolayer. Based on this sample, exact cell number calculated according to µl as 1466 cells/ µl. 15 µl loading volume can be enough for flow channel so 22000 cells/ 15 µl obtained by multiplying of 1466 cells/ µl with 15 µl. This number rounded up to 30000 cells/ 15 µl and tried for further endothelial monolayer formation experiment. It worked in chip consists of 1 mm width x 381 µm height and number was optimized 7500000 cells/ml for this chip. (Figure 3.12) Then this was repeated for different chips in different height and it worked. Finally it was optimized as 19650 cell/µm to be identical for any height of master mold.

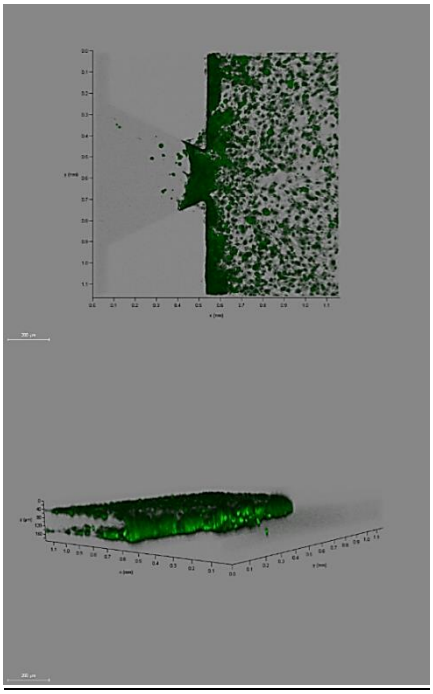

Figure 3.9. $20x10^6$ endothelial cell restructuring with poli-L-lysine and fibronectin coating prior to loading the cells in different positions

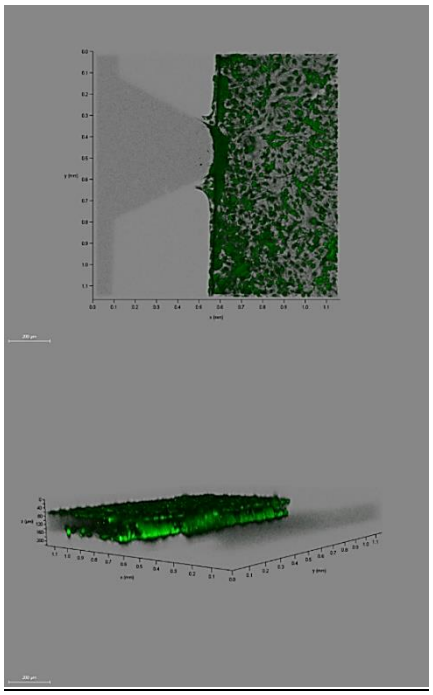

Figure 3.10. $20x10^6$ endothelial cell restructuring with APTES and fibronectin coating prior to loading the cells in different positions. Scale Bar: 200 μm.

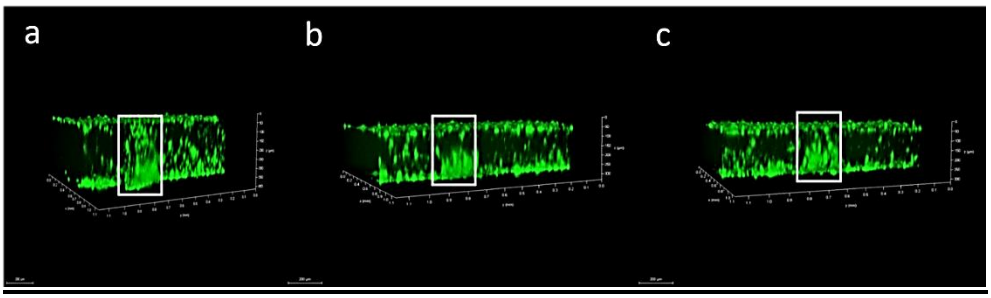

Figure 3.11. $7.5x10^6$ cell loading into device coated with various proteins at same concentrations. a)0.0125 mg/ml collagen Type I b)0.0125 mg/ml fibronectin c) 0.0125 mg/ml laminin.

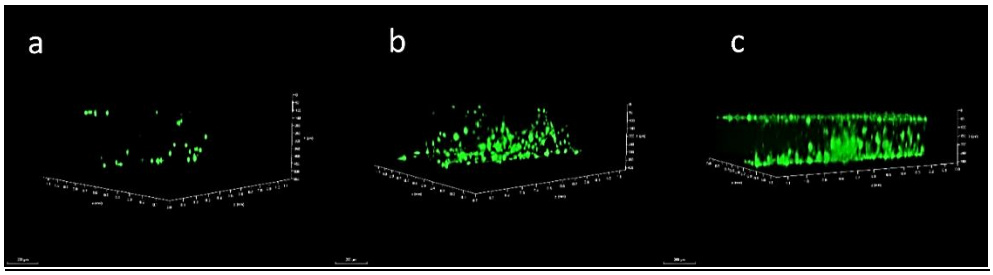

Figure 3.12. Cell number trial for endothelial monolayer formation. a)110000 cells/ml, b) 1500000 cells/ml c)7500000 cells/ml

3.4. Permeability Assessment of Endothelial Monolayer during Hypoxia and Normoxia in Dynamic and Static Conditions

To assess endothelial monolayer integrity among static, flow and hypoxia conditions. As shown Figure 3.13 and Figure 3.14, hypoxic exposure and flow triggers vascular permeability in static conditions during 30 minutes. However, no significance was observed among normoxia and hypoxia samples within 1 minute although normoxia and hypoxia samples showed significance with no endothelial monolayer condition within 1 minute (Figure 3.15). According to Figure 3.16, normoxia and severe hypoxia (4 hour) have more significance with no endothelial barrier condition than mild hypoxia(6 hour) in static condition during 30 minute (***=$p<0.001$, **= $p<0.01$). However, when flow considered addition to hypoxia, it affects permeability more much when compared to static and hypoxic conditions. (Figure 3.14) As a result, the perfusion flow reshape the vascular geometry more than static and hypoxic conditions even if no significance observed between normoxia and hypoxia conditions in static conditions.

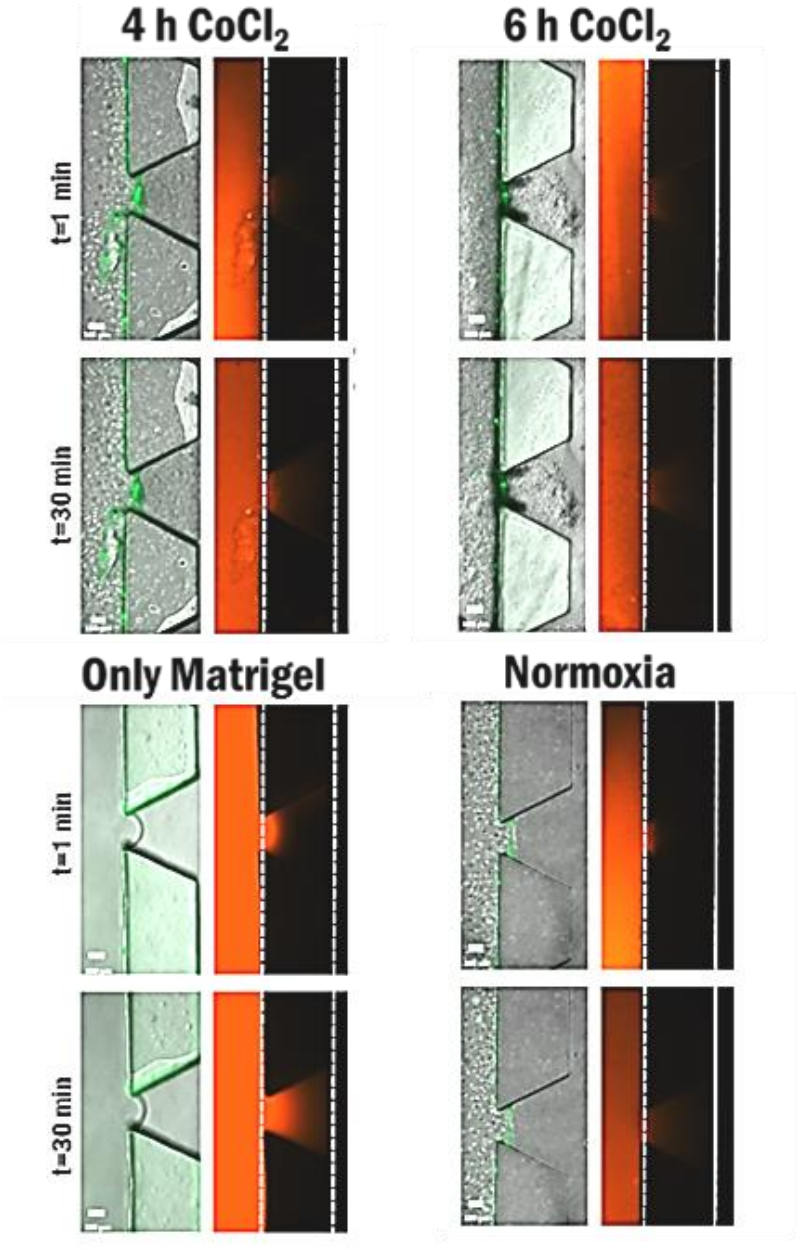

Figure 3.13. 70 kDa TMR dextran diffusion across endothelial monolayer at 1 and 30 minute under static condition. only matrigel=without endothelial monolayer. Scale Bar: 100 μM

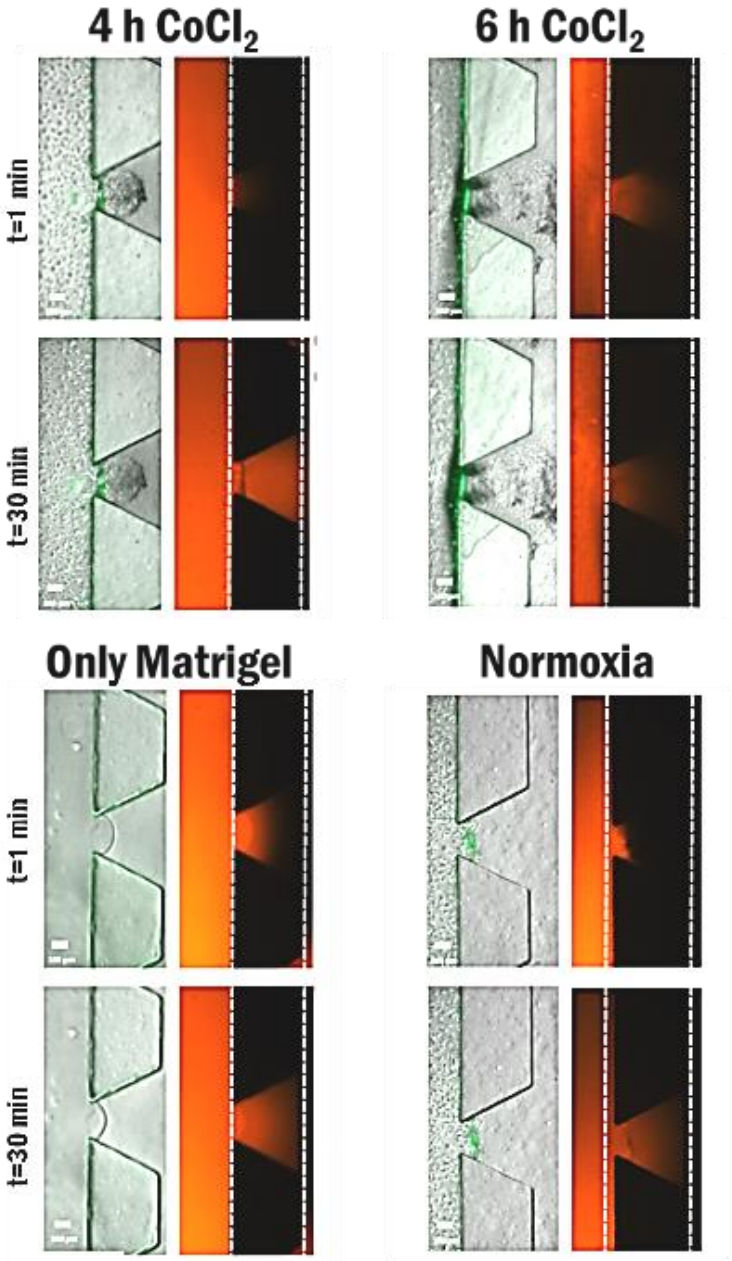

Figure 3.14. 70 kDa TMR dextran diffusion across endothelial monolayer at 1 and 30 minute with 0.77 dyne/cm^2. only matrigel=without endothelial monolayer. Scale Bar: 100 μM

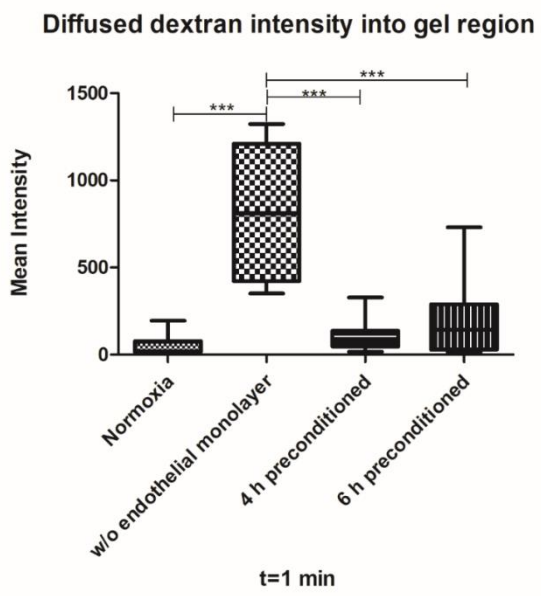

Figure 3.15. 70 kDa TMR dextran diffusion across endothelial monolayer to gel region at 1 minute normoxia, severe (4 hour) and mild (6 hour) hypoxia and without endothelial monolayer. ***=p<0.001

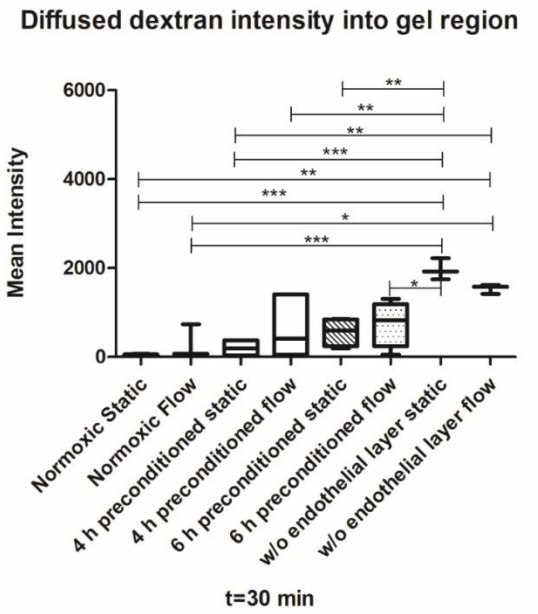

Figure 3.16. 70 kDa TMR dextran diffusion across endothelial monolayer to gel region at 30 minutes normoxia, severe (4 hour) and mild (6 hour) hypoxia and without endothelial monolayer with perfusion flow and without perfusion flow ***=p<0.001

3.5. Extravasated Particle and Metric Quantification

Regarding hypoxia, it can be neglected in intact monolayer in static conditions. However, MCF10A in severe (4 hour) hypoxia with perfusion flow behaves more extravasation than mild hypoxia (6 hour) (Figure 3.17). In addition to these, extravasation metric shows hypoxia should be considered between samples in intact monolayer. Since, There are significance among samples in terms of hypoxia, perfusion flow and cell lines regarding of intact monolayer (Figure 3.18).

Although extravasation metric of normoxia and hypoxia samples in static are similar, the significance are observed between them in terms of particle when considering intact and nonintact monolayer (Figure 3.19, Figure 3.20). In addition to these, Flow decreases extravasation both in normoxia and hypoxia considering extravasation metric. In fact, hypoxia with perfusion flow is much more powerful than they applied separately regarding MDAMB231 although MCF10A extravasation seemed to increase with hypoxia with perfusion flow (Figure 3.20).

In extravasation event, as shown Figure 3.19, MDAMB231 was observed more much migration across endothelial monolayer under normoxic and static condition when compared to 4 hour hypoxic circumstance.($p<0.05$). Besides, significant decrease in extravasated cell number was observed in normoxia between static and flow condition.($p<0.05$). Both hypoxia and flow exposure showed same situation when compared to normoxic and static condition but more significant decreasing can be seen both in 4 hours hypoxia and flow comparing to normoxia under static condition. ($p<0.01$).

In addition to these, both hypoxia and flow applied triggers MCF10A extravasation. However, they have no significant increasing within MCF10A conditions include normoxia, static and flow (Figure 3.19). Nevertheless, when compared to 4 hours hypoxia in flow, MCF10A extravasation was greater than MDAMB231 as shown Figure 3.19. ($p<0.05$)

Regarding intact monolayer, Extravasation seems cell and perfusion based even if associated cells are taken into account between hypoxia and normoxia (Figure 3.21). However, as shown in Figure 3.19 and Figure 3.22, they are pretty same both extravasation and association in intact and non intact monolayer. That's why, associated cells can be included for extravasation analysis. For clear interpretation

between hypoxia and normoxia, all inputs should be taken into account for extravasation because vascular geometry influences the extravasation caused by hypoxia and perfusion flow.

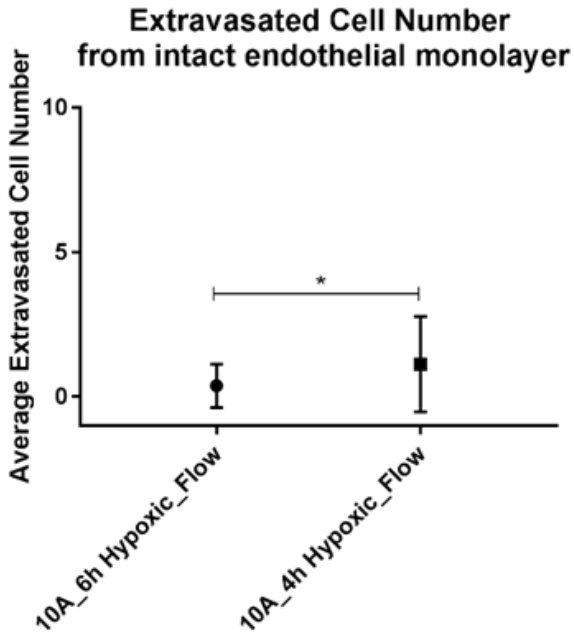

Figure 3.17. Average extravasated cell number from intact endothelial monolayer. *=p<0.05

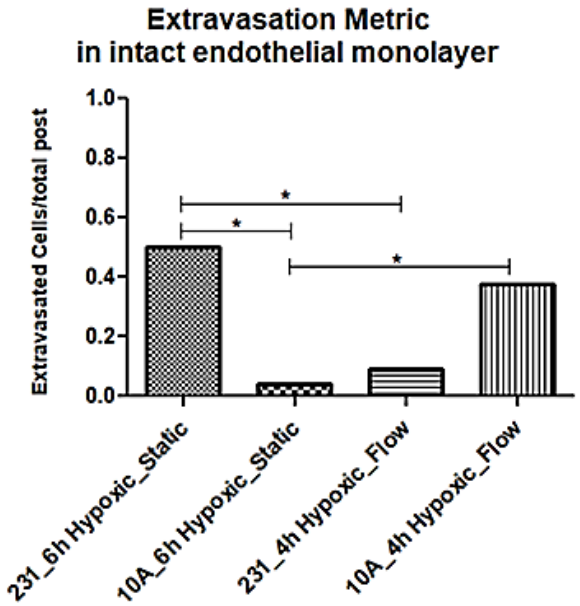

Figure 3.18. Extravasation metric in intact endothelial monolayer. *=p<0.05

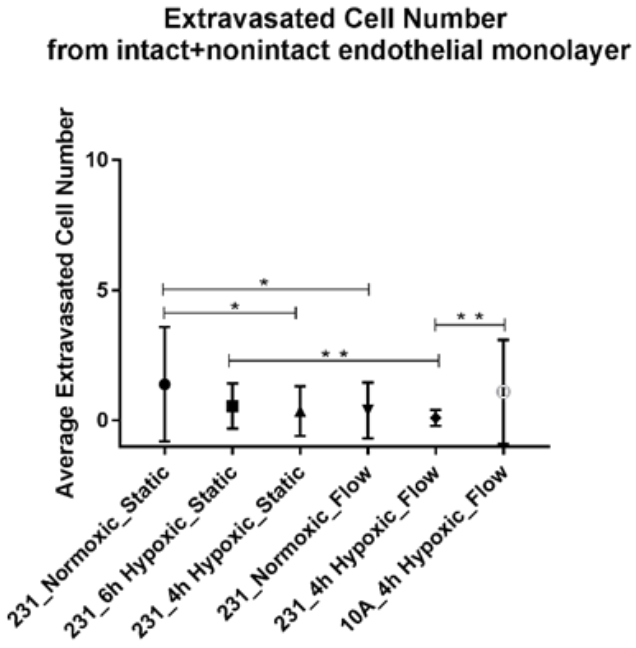

Figure 3.19. Average extravasated cell number from intact and nonintact endothelial monolayer. *=p<0.05, **=p<0.01

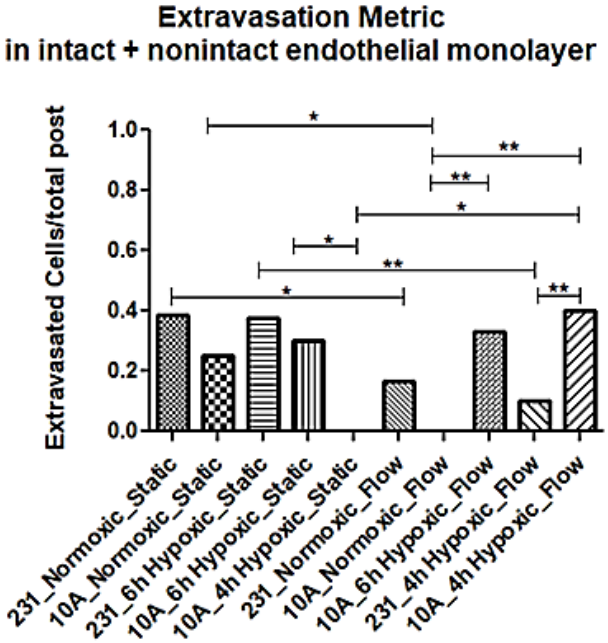

Figure 3.20. Extravasation metric in intact and nonintact endothelial monolayer. *=p<0.05, **=p<0.01

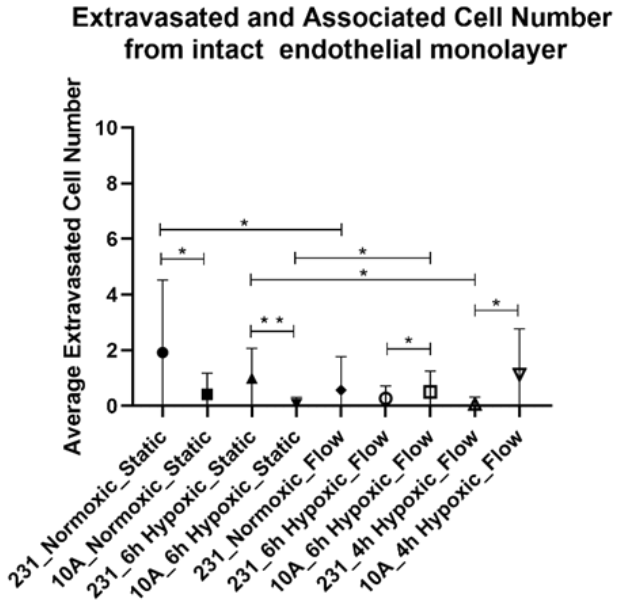

Figure 3.21. Average extravasated and associated cell number from intact endothelial monolayer. *=p<0.05, **=p<0.01

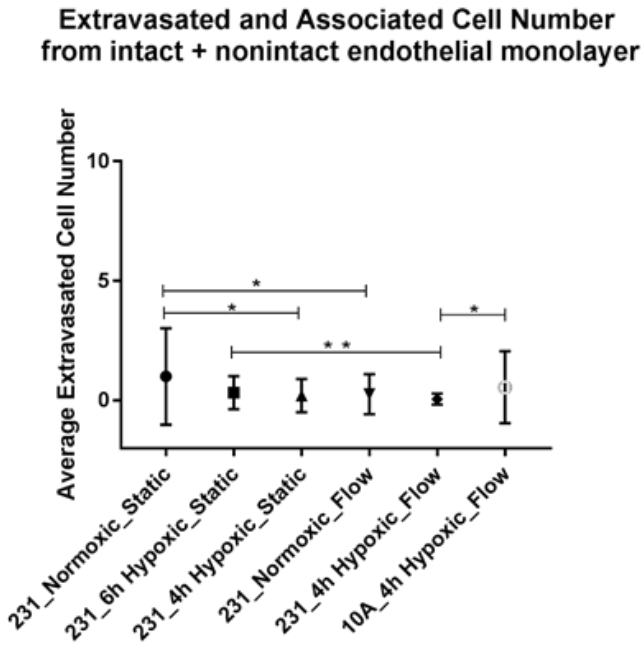

Figure 3.22. Average extravasated and associated cell number from intact and nonintact endothelial monolayer. *=p<0.05, **=p<0.01

3.6. Determination of Extravasated Cell Distance

Once circulated cells extravasated, it must be known that how far they are in extracellular matrix/tissue/organ for further observation such as localization, tumor formation etc. As shown Figure 3.23, flow throws MDAMB231 away in normoxia when compared to static conditions.($p<0.05$). Once again shown Figure 3.23, regarding MDAMB231, normoxia with perfusion flow is more powerful than mild hypoxia(6 hour) with perfusion flow at a distance($p>0.05$). Besides, hypoxia with perfusion flow directed MDAMB231 extravasation less than normoxia with perfusion flow in terms of both intact and intact/nonintact endothelial monolayer. Migration of MDAMB231 over endothelial monolayer in hypoxia without perfusion flow much more higher than MDAMB231 migrated in normoxia without perfusion flow (Figure 3.23, Figure 3.24). It shows migration over endothelial monolayer in hypoxia without perfusion flow is tightly associated with intact endothelial monolayer. In terms of static conditions, MDAMB231 extravasated forward more in 6 hours hypoxia than in normoxia but this result is not significant. However, Figure 3.16 shows that extravasation distance may be directed with flow in normoxia over hypoxia.

Regarding MCF10A, it goes away in 6 hours hypoxia under flow conditions over 4 hours hypoxia as shown Figure 3.23.($p<0.05$) Although MCF10A extravasated away in 6 hours hypoxia when compared to 6 hours flow condition but they are not significant from each other. Besides, when compared to MDAMB231, MCF10A extravasated further away in 6 hours hypoxia under flow condition. ($p<0.05$)

In addition to these, distance migration is important for ending of extravasation, localization of malignant cells and eventually micro and macro tumor formation. According to our models, once cells extravasate both in hypoxia and normoxia, it can not form a tumor in extracellular matrix (Figure A.8). However, it is not valid everytime because tumor microenvironment is quite complex and requires more much inputs for permitting tumor formation.

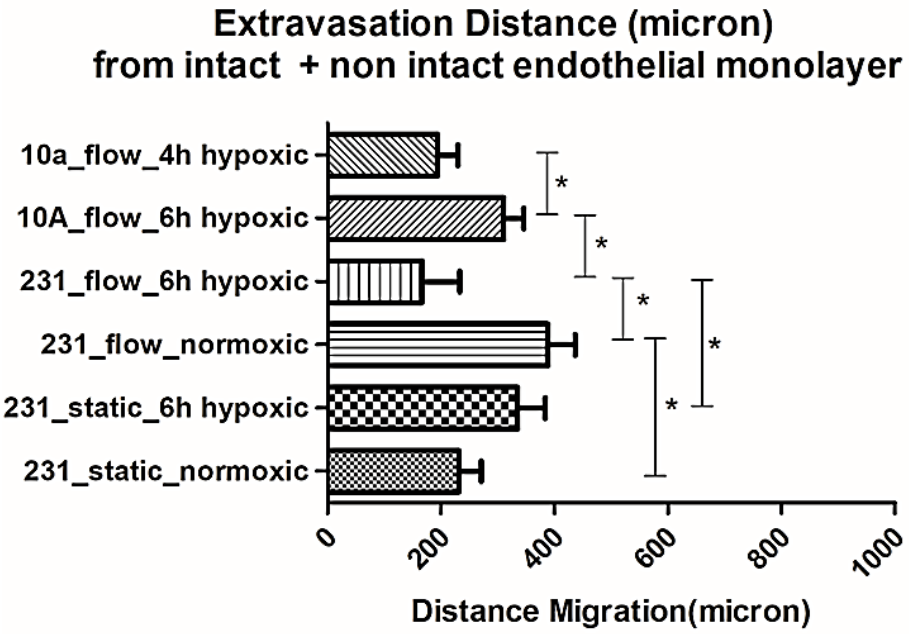

Figure 3.23. Extravasated cell distance across intact and nonintact endothelial monolayer *=p<0.05

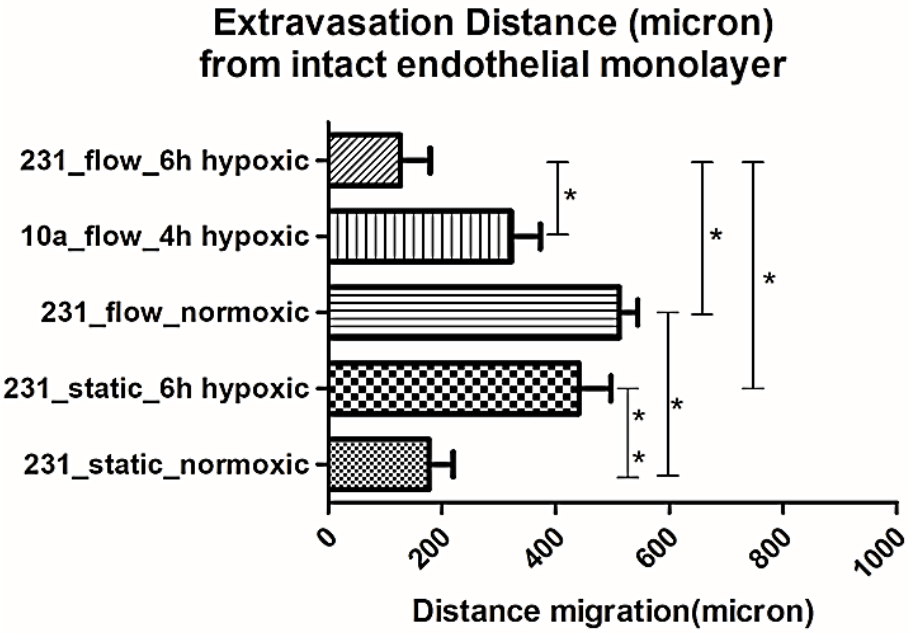

Figure 3.24. Extravasated cell distance across intact endothelial monolayer *=p<0.05, **=p<0.01

CHAPTER 4

DISCUSSIONS

According to our results, vascular permeability is changing with flow rather than hypoxia (Figure 3.14, Figure 3.15 and Figure 3.16). Hypoxia change the vascular geometry nonsignificantly when compared to normoxia (Figure 3.13, Figure 3.15 and Figure 3.16). Nevertheless, mean intensity in the gel region is ascending increasingly from normoxia to hypoxia and number of nonintact endothelial monolayer in hypoxia are more much than normoxia (Figure A.9).

In extravasation event, we tried to evaluate from a broad perspective as particle, metric, distance and state of intact monolayer. As expected MDAMB231 extravasated into extracellular matrix more in static condition comparing with flow. Indeed, we were thinking MDAMB231 to extravasate a little bit in normoxia than hypoxia. Since, vascular permeability is supposed to increase during hypoxia and it allows malignant cells to introduce with extracellular matrix/tissue/organ. According to our results, less extravasation in hypoxia can be caused by cell viability of MDAMB231 and MCF10A agains cobalt treatment. According to viability results, MCF10A is more viable than MDAMB231 in 100μm $CoCl_2$ and its extravasation is expected much more than MDAMB231 do. However, MDAMB231 extravasated much more than MCF10A in static conditions because extravasation is cell based in these cases. Nevertheless, we faced opposite results against previously stated papers[12,30,31] According to [31], they found significant extravasation in hypoxia but they set up different experimental conditions apart from us. For instance, they preconditioned MDAMB231, MCF10A and MCF7 prior to vasculature formation. They found that extravasated cell number varies from hypoxia to normoxia. Surprisingly, they revealed that MCF10A extravasation greater than MDAMB231 in hypoxia. Actually this results overlap with our results. They suggest MCF10A transforms their phenotype by expressing vimentin during hypoxic exposure [31]. A paper stated same outcome as previously described [47]. However, we revealed that MCF10A extravasation is not only depend on hypoxia but also in relation with flow. We have clearly seen much more extravasation of MCF10A in hypoxia under

dynamic conditions which involved in applying flow. However, MCF10A and its hypoxic response is still poorly understood because of endothelial monolayer preconditioning with cobalt chloride before introducing of MCF10A into channels. According to previous paper [6], they proposed that E-selectin and MCF10A , extravasation and MCF10A relation is directly proportional. Hypoxia gives rise to inducing E-selectin from endothelial cells to permit cell adhesion[12] .Additionally they stated that MCF10A migration speed is faster than MDAMB231 and MCF10A is travelling like circular or follow any irregular axis. unlike the linear straight road where MDAMB231 follow [6] . Actually these findings support to our results because we found MCF10A has gone away as much as possible comparing with MDAMB231 in 6 hour hypoxia with flow. Similarly, our findings are controversial to previous research as well. They found hypoxia induced breast cancer cell extravasation to lung [30]. However, in our system, we have just measure how well extravasation occurs in extracellular matrix without any tissue in hypoxia. They have already measure effects of some specific genes like angiopoietin-like-4 triggered by hypoxia on extravasation. However, even if it is conducted in vivo, they also show effects of chemokine secreted by lung on metastasis in hypoxia. Another paper defending positive relation between hypoxia and extravasation suggest that as HIF1 is depleted in endothelial cells, some other type of HIF can be activated and this situation can turn the tables in terms of metastasis [12].Apart from these our results fit into some papers previously described [16,32,33]. Taken together and our results, metastasis requires a lot of elements to drive breast cancer cell extravasation. Apart from HIF1, some hypoxic elements can suppress extravasation of cancer cells.

Additionally, both MDAMB231 and MCF10A tend to go away as expected during hypoxia under static conditions because they want to reach and degrade matrigel/collagen through lysyl oxidase induced by HIF1 [19,22]. However, we revealed that applied perfusion flow is much more effective way to throw cells away when compared to transition to hypoxia.

CHAPTER 5

CONCLUSION

In this study, we tried to investigate HIF1α dependent extravasation mechanism into extracellular matrix with dynamic perfusion and without dynamic perfusion. Lab-on-a chip devices allowed us to working on it in three dimensional micro environment. Indeed, we could generate blood vessel like structure with dynamic perfusion mimicking blood flow by means of innate multidisciplinary of microfluidics within this context.

We have clearly see how endothelial monolayer disrupted with perfusion flow. We are supposed to see more extravasation in relation with metastatic efficiency of endothelial monolayer structure in hypoxia. However, malignant cells extravasate more much in normoxia considering hypoxia in a way although HIF1α activated endothelial monolayer gave permission to cancer cells to extravasation. As dynamic perfusion minimize the extravasated cell number, they make the extravasation possible more without dynamic perfusion. Moreover, dynamic perfusion assists that as MDAMB231 is stepping out more in normoxia, MCF10A is going away more in hypoxia. Both of them are extravasated further through flow comparing to static condition.

All in all, there are the questions in the wide range to be answered about hypoxia and extravasation mechanism. Precise and proper in vivo and / or fully mimicked three dimensional studies will clarify underlying mechanism on these. Nevertheless this is multistep process and cell to cell, cell to matrix and subcellular molecular pathways are absolutely necessary for unanswered questions.

REFERENCES

[1] https://www.who.int/news-room/fact-sheets/detail/cancer

[2] Hanahan, Douglas, and Robert A Weinberg. 2011. “Hallmarks of Cancer: The next Generation.” Cell 144 (5): 646–74. https://doi.org/10.1016/j.cell.2011.02.013.

[3] Weinberg, Chaffer and. 2013. “A Perspective on Cancer Metastasis.” Nature Medicine 19 (2): 179–92. https://doi.org/10.1126/science.1203543.

[4] Qu, Ying, Bingchen Han, Yi Yu, Weiwu Yao, Shikha Bose, Beth Y. Karlan, Armando E. Giuliano, and Xiaojiang Cui. 2015. “Evaluation of MCF10A as a Reliable Model for Normal Human Mammary Epithelial Cells.” PLoS ONE 10 (7): 1–16. https://doi.org/10.1371/journal.pone.0131285.

[5] Lanz, Henriette L., Anthony Saleh, Bart Kramer, Junmei Cairns, Chee Ping Ng, Jia Yu, Sebastiaan J. Trietsch, et al. 2017. “Therapy Response Testing of Breast Cancer in a 3D High-Throughput Perfused Microfluidic Platform.” BMC Cancer 17 (1): 1–11. https://doi.org/10.1186/s12885-017-3709-3.

[6] Agus, David B., Jenolyn F. Alexander, Wadih Arap, Shashanka Ashili, Joseph E. Aslan, Robert H. Austin, Vadim Backman, et al. 2013. “A Physical Sciences Network Characterization of Non-Tumorigenic and Metastatic Cells.” Scientific Reports 3. https://doi.org/10.1038/srep01449.

[7] Ebbesen, Erik O. Pettersen, Juliana, Peter. 2002. “Hypoxia, Normoxia and Hyperoxia: Terminology for Medical In Vitro Cell Biology.” Acta Oncologica 39 (2): 247–48. https://doi.org/10.1080/028418600430888.

[8] McKeown, S. R. 2014. “Defining Normoxia, Physoxia and Hypoxia in Tumours - Implications for Treatment Response.” British Journal of Radiology 87 (1035): 1–12. https://doi.org/10.1259/bjr.20130676.

[9] Harris, Adrian L. 2002. “Hypoxia — a Key Regulatory Factor in Tumour Growth.” Nature Reviews Cancer 2 (1): 38–47. https://doi.org/10.1038/nrc704.

[10] Zheng, Jie. 2012. “Energy Metabolism of Cancer: Glycolysis versus Oxidative Phosphorylation (Review).” Oncology Letters 4 (6): 1151–57. https://doi.org/10.3892/ol.2012.928.

[11] Wong, Carmen Chak Lui, Alan Ka Lun Kai, and Irene Oi Lin Ng. 2014. “The Impact of Hypoxia in Hepatocellular Carcinoma Metastasis.” Frontiers of Medicine in China 8 (1): 33–41. https://doi.org/10.1007/s11684-013-0301-3.

[12] Evans, Colin E., Cristina Branco-Price, and Randall S. Johnson. 2012. “HIF-Mediated Endothelial Response during Cancer Progression.” International Journal of Hematology 95 (5): 471–77. https://doi.org/10.1007/s12185-012-1072-3.

[13] Zhang, Yan Bo, Xiulian Wang, Edward A. Meister, Ke Rui Gong, Shao Chun Yan, Guo Wei Lu, Xun Ming Ji, and Guo Shao. 2014. “The Effects of CoCl2 on HIF-1α Protein under Experimental Conditions of Autoprogressive Hypoxia Using Mouse Models.” International Journal of Molecular Sciences 15 (6): 10999–12. https://doi.org/10.3390/ijms150610999.

[14] Kim, So Young, Yong Jun Choi, Sun Myung Joung, Byung Ho Lee, Yi Sook Jung, and Joo Young Lee. 2010. “Hypoxic Stress Up-Regulates the Expression of Toll-like Receptor 4 in Macrophages via Hypoxia-Inducible Factor.” Immunology 129 (4): 516–24. https://doi.org/10.1111/j.1365-2567.2009.03203.x.

[15] Yuan, Yong, George Hilliard, Tsuneo Ferguson, and David E. Millhorn. 2003. “Cobalt Inhibits the Interaction between Hypoxia-Inducible Factor-α and von Hippel-Lindau Protein by Direct Binding to Hypoxia-Inducible Factor-α.” Journal of Biological Chemistry 278 (18): 15911–16. https://doi.org/10.1074/jbc.M300463200.

[16] Galaup, A., A. Cazes, S. Le Jan, J. Philippe, E. Connault, E. Le Coz, H. Mekid, et al. 2006. “Angiopoietin-like 4 Prevents Metastasis through Inhibition of Vascular Permeability and Tumor Cell Motility and Invasiveness.” Proceedings of the National Academy of Sciences 103 (49): 18721–26. https://doi.org/10.1073/pnas.0609025103.

[17] Semenza, G. L. 2013. “Cancer-Stromal Cell Interactions Mediated by Hypoxia-Inducible Factors Promote Angiogenesis, Lymphangiogenesis, and Metastasis.” Oncogene 32 (35): 4057–63. https://doi.org/10.1038/onc.2012.578.

[18] Sullivan, Richard, and Charles H. Graham. 2007. “Hypoxia-Driven Selection of the Metastatic Phenotype.” Cancer and Metastasis Reviews 26 (2): 319–31. https://doi.org/10.1007/s10555-007-9062-2.

[19] Semenza, Gregg L. 2012. “Molecular Mechanisms Mediating Metastasis of Hypoxic Breast Cancer Cells.” Trends in Molecular Medicine 18 (9): 534–43. https://doi.org/10.1016/j.molmed.2012.08.001.

[20] West, John B. 2017. “Physiological Effects of Chronic Hypoxia.” New England Journal of Medicine 376 (20): 1965–71. https://doi.org/10.1056/nejmra1612008.

[21] Funamoto, Kenichi, Daisuke Yoshino, Kento Matsubara, Ioannis K. Zervantonakis, Kiyoe Funamoto, Masafumi Nakayama, Jun Masamune, Yoshitaka Kimura, and Roger D. Kamm. 2017. “Endothelial Monolayer Permeability under Controlled Oxygen Tension.” Integrative Biology (United Kingdom) 9 (6): 529–38. https://doi.org/10.1039/c7ib00068e.

[22] Erler, Janine T., Kevin L. Bennewith, Thomas R. Cox, Georgina Lang, Demelza Bird, Albert Koong, Quynh Thu Le, and Amato J. Giaccia. 2009. “Hypoxia-Induced Lysyl Oxidase Is a Critical Mediator of Bone Marrow Cell Recruitment to Form the Premetastatic Niche.” Cancer Cell 15 (1): 35–44. https://doi.org/10.1016/j.ccr.2008.11.012.

[23] Bayer, Christine, Kuangyu Shi, Sabrina T. Astner, Constantin-Alin Maftei, and Peter Vaupel. 2011. “Acute Versus Chronic Hypoxia: Why a Simplified Classification Is Simply Not Enough.” International Journal of Radiation Oncology*Biology*Physics 80 (4): 965–68. https://doi.org/10.1016/j.ijrobp.2011.02.049.

[24] Vaupel, Peter, Arnulf Mayer, Susanne Briest, and Michael Höckel. 2005. “Hypoxia in Breast Cancer: Role of Blood Flow, Oxygen Diffusion Distances, and Anemia in the Development of Oxygen Depletion.” Advances in Experimental Medicine and Biology 566: 333–42. https://doi.org/10.1007/0-387-26206-7_44.

[25] Varlotto, John, and Mary Ann Stevenson. 2005. “Anemia, Tumor Hypoxemia, and the Cancer Patient.” International Journal of Radiation Oncology Biology Physics 63 (1): 25–36. https://doi.org/10.1016/j.ijrobp.2005.04.049.

[26] Danon, Abraham, and Georges Assouline. 1979. “Antiulcer Activity of Hypertonic Solutions in the Rat: Possible Role of Prostaglandins.” European

Journal of Pharmacology 58 (4): 425–31. https://doi.org/10.1016/0014-2999(79)90313-3.

[27] Vaupel, Peter, and Arnulf Mayer. 2016. “Oxygen Transport to Tissue XXXVII” 876: 19–24. https://doi.org/10.1007/978-1-4939-3023-4.

[28] Katt, Moriah E., Amanda L. Placone, Andrew D. Wong, Zinnia S. Xu, and Peter C. Searson. 2016. “In Vitro Tumor Models: Advantages, Disadvantages, Variables, and Selecting the Right Platform.” Frontiers in Bioengineering and Biotechnology 4 (February). https://doi.org/10.3389/fbioe.2016.00012.

[29] Aziz, Aziz, Chunyang Geng, Mengjie Fu, Xiaohui Yu, Kairong Qin, and Bo Liu. 2017. “The Role of Microfluidics for Organ on Chip Simulations.” Bioengineering 4 (4): 39. https://doi.org/10.3390/bioengineering4020039.

[30] Zhang, H., C. C.L. Wong, H. Wei, D. M. Gilkes, P. Korangath, P. Chaturvedi, L. Schito, et al. 2012. “HIF-1-Dependent Expression of Angiopoietin-like 4 and L1CAM Mediates Vascular Metastasis of Hypoxic Breast Cancer Cells to the Lungs.” Oncogene 31 (14): 1757–70. https://doi.org/10.1038/onc.2011.365.

[31] Song, Jiho, Agnès Miermont, Chwee Teck Lim, and Roger D. Kamm. 2018. “A 3D Microvascular Network Model to Study the Impact of Hypoxia on the Extravasation Potential of Breast Cell Lines.” Scientific Reports 8 (1): 1–11. https://doi.org/10.1038/s41598-018-36381-5.

[32] Subarsky, Patrick, and Richard P. Hill. 2008. “Graded Hypoxia Modulates the Invasive Potential of HT1080 Fibrosarcoma and MDA MB231 Carcinoma Cells.” Clinical and Experimental Metastasis 25 (3): 253–64. https://doi.org/10.1007/s10585-007-9139-x.

[33] Sun, Li, Yang Liu, Sensen Lin, Jing Shang, Jin Liu, Ji Li, Shengtao Yuan, and Luyong Zhang. 2013. “Early Growth Response Gene-1 and Hypoxia-Inducible Factor-1α Affect Tumor Metastasis via Regulation of Tissue Factor.” Acta Oncologica 52 (4): 842–51. https://doi.org/10.3109/0284186X.2013.705890.

[34] Ozdil, Berrin, Sevgi Onal, Tugce Oruc, and Devrim Pesen Okvur. 2014. “Fabrication of 3D Controlled in Vitro Microenvironments.” MethodsX 1 (1): 60–66. https://doi.org/10.1016/j.mex.2014.06.003.

[35] Siddique, Asma, Tobias Meckel, Robert W. Stark, and Suman Narayan. 2017. “Improved Cell Adhesion under Shear Stress in PDMS Microfluidic Devices.”

Colloids and Surfaces B: Biointerfaces 150: 456–64. https://doi.org/10.1016/j.colsurfb.2016.11.011.

[36] Spiegel, Asaf, Mary W Brooks, Samin Houshyar, Ferenc Reinhardt, Michele Ardolino, Evelyn Fessler, Michelle B Chen, et al. 2017. “HHS Public Access” 6 (6): 630–49. https://doi.org/10.1158/2159-8290.CD-15-1157.Neutrophils.

[37] Tran, Reginald, Elaissa Trybus Hardy, Michelle Tsai, Wilbur A. Lam, Ashley Kita, Byungwook Ahn, Robert Mannino, Yumiko Sakurai, and David R. Myers. 2012. “Endothelialized Microfluidics for Studying Microvascular Interactions in Hematologic Diseases.” Journal of Visualized Experiments, no. 64: 8–11. https://doi.org/10.3791/3958.

[38] Bischel, Lauren L, Edmond W K Young, Brianah R Mader, and David J Beebe. 2014. “Tubeless Microfluidic Angiogenesis Assay With Three- Dimensional Endothelial-Lined Microvessels.” Biomaterials 34 (5): 1471–77. https://doi.org/10.1016/j.biomaterials.2012.11.005.Tubeless.

[39] Morier, Patrick, Christine Vollet, Philippe E. Michel, Frédéric Reymond, and Joël S. Rossier. 2004. “Gravity-Induced Convective Flow in Microfluidic Systems: Electrochemical Characterization and Application to Enzyme-Linked Immunosorbent Assay Tests.” Electrophoresis 25 (21–22): 3761–68. https://doi.org/10.1002/elps.200406093.

[40] Bruus, Henrik. 2007. “Theoretical Microfluidics (Oxford Master Series in Physics)” 18. https://doi.org/10.1017/CBO9781107415324.004.

[41] Paszkowiak, Jacek J., and Alan Dardik. 2003. “Arterial Wall Shear Stress: Observations from the Bench to the Bedside.” Vascular and Endovascular Surgery 37 (1): 47–57. https://doi.org/10.1177/153857440303700107.

[42] Jeon, Jessie S., Ioannis K. Zervantonakis, Seok Chung, Roger D. Kamm, and Joseph L. Charest. 2013. “In Vitro Model of Tumor Cell Extravasation.” PLoS ONE 8 (2). https://doi.org/10.1371/journal.pone.0056910.

[43] Manley, Gerard, Jason R. Conn, Elizabeth M. Catchpoole, Naomi Runnegar, Sally J. Mapp, and Kate A. Markey. 2017. “Public Access NIH Public Access.” PLoS ONE 32 (7): 736–40. https://doi.org/10.1371/journal.pone.0178059.

[44] Bersini, S, Jeon J.S., Dubini, G, Arrigoni, C, Chung, S, Charest, J.L., Moretti, M., Kamm, R.D. 2014. “NIH Public Access.” Biomaterials 35 (8): 2454–61. https://doi.org/10.1016/j.pestbp.2011.02.012.Investigations.

[45] Lee, Philbert, and Xiaoyang Wu. 2015. “Review: Modifications of Human Serum Albumin and Their Binding Effect.” Current Pharmaceutical Design 21 (14): 1862–65.

[46] Csete, M. 1998. “Cellular Response to Hypoxia.” Anesthesiology Clinics of North America 16 (1): 201–10. https://doi.org/10.1016/S0889-8537(05)70014-6.

[47] Vaapil, Marica, Karolina Helczynska, René Villadsen, Ole W. Petersen, Elisabet Johansson, Siv Beckman, Christer Larsson, Sven Påhlman, and Annika Jögi. 2012. “Hypoxic Conditions Induce a Cancer-Like Phenotype in Human Breast Epithelial Cells.” PLoS ONE 7 (9). https://doi.org/10.1371/journal.pone.0046543.

APPENDIX A

SUPPLEMENTARY FIGURES

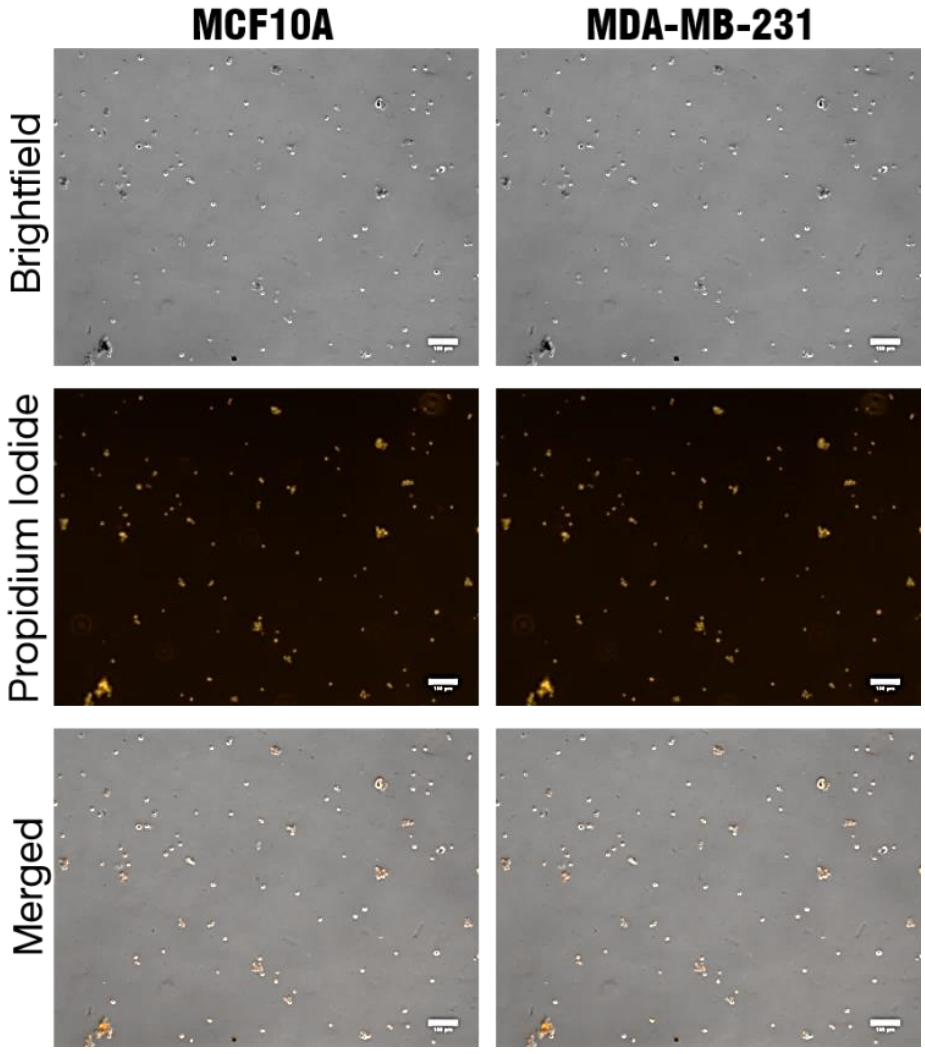

Figure A.1. MDAMB231 and MCF10A viabilities when they preconditioned in non treated petri dish 100 µM $CoCl_2$ for 6 hour. (propidium iodide shows dead cells). Scale Bar= 100 µm.

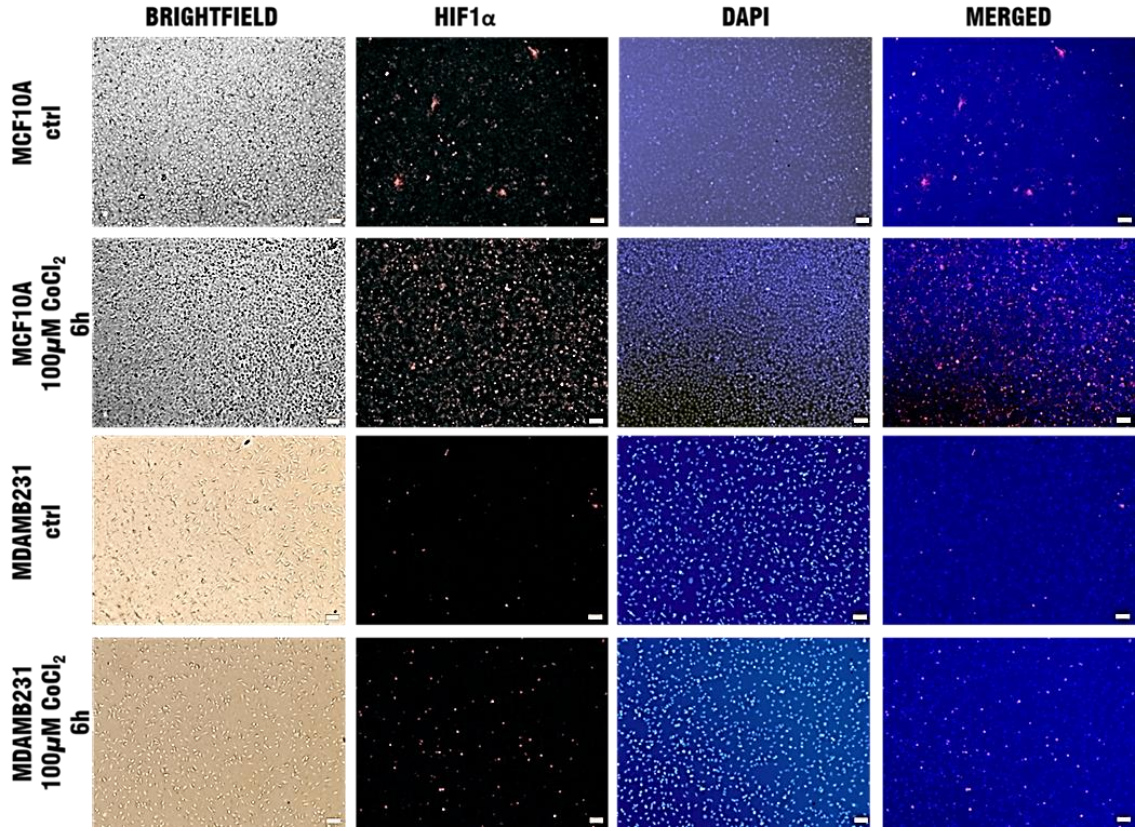

Figure A.2. An image showing HIF1α localization in nuclei of MDAMB231 and MCF10A when 100 μM $CoCl_2$ applied for 6 hour. Scale Bar= 100 μm.

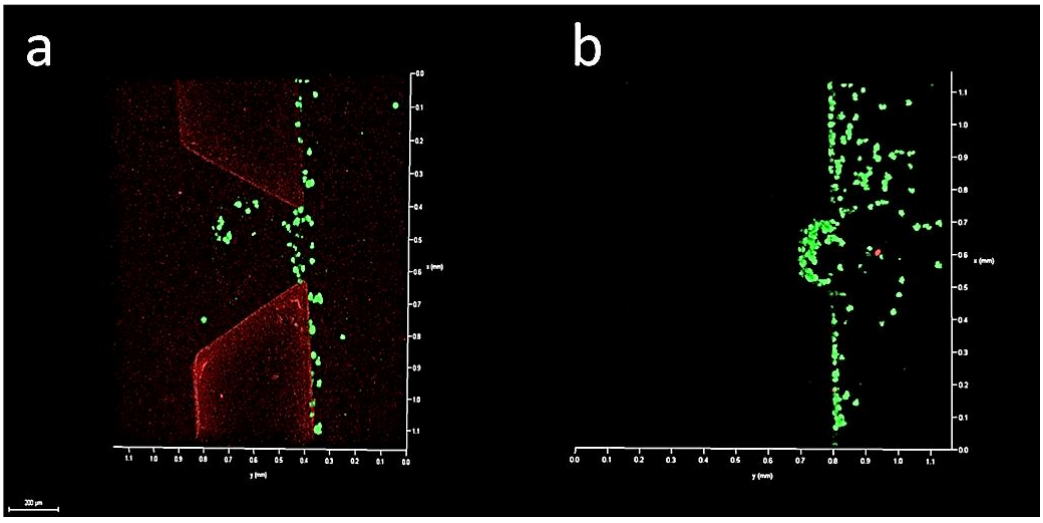

Figure A.3. State of circulated cells to be loaded into flow channel for observing extravasation event. a)10000 cells/ml b)20000 cells/ml. Scale Bar: 200 μm

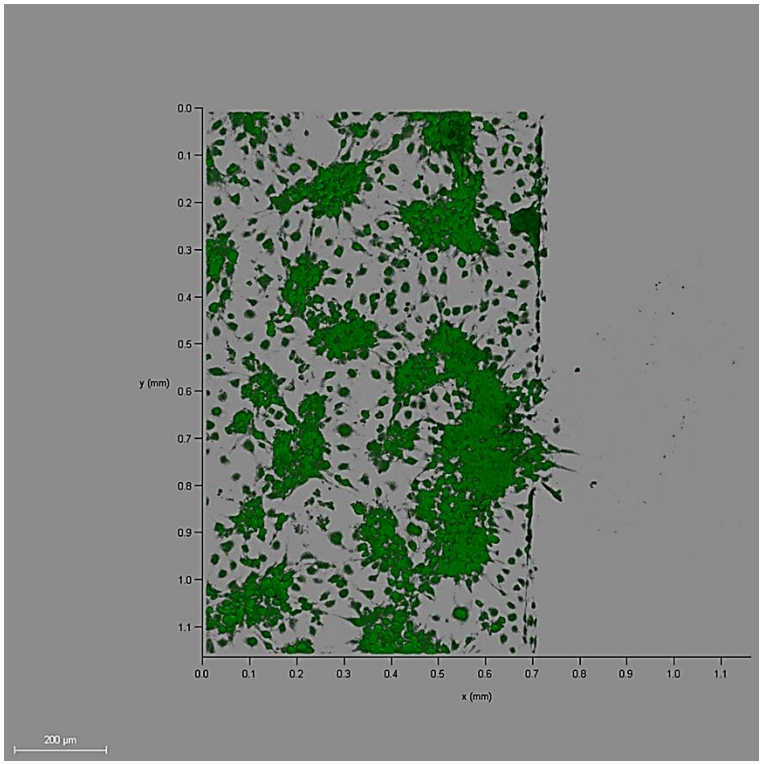

Figure A.4. Top view of endothelial monolayer without 8%450-650 kDa dextran. Scale Bar: 200 µm

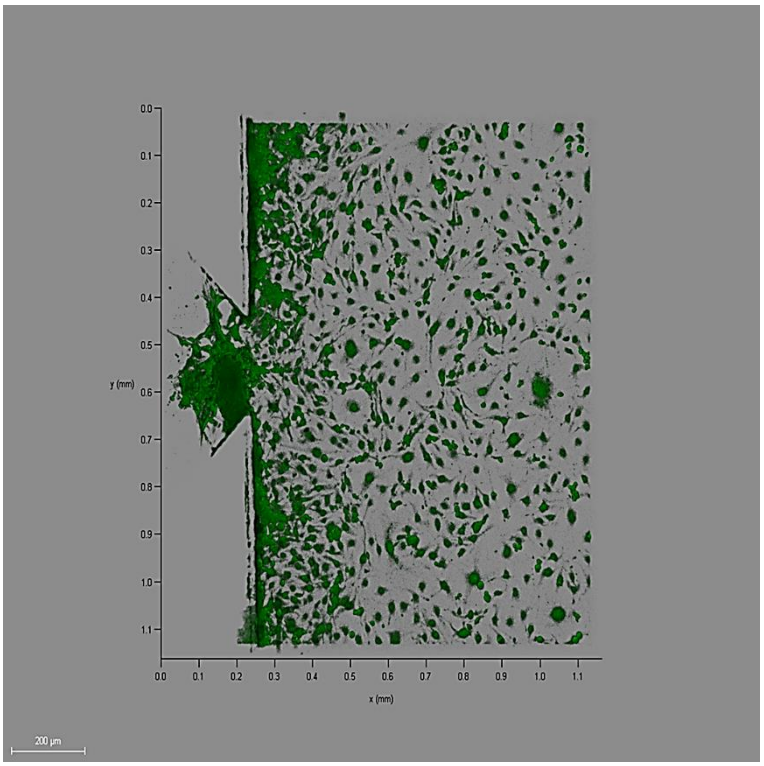

Figure A.5. Top view of endothelial monolayer with 8%450-650 kDa dextran. Scale Bar: 200 µm

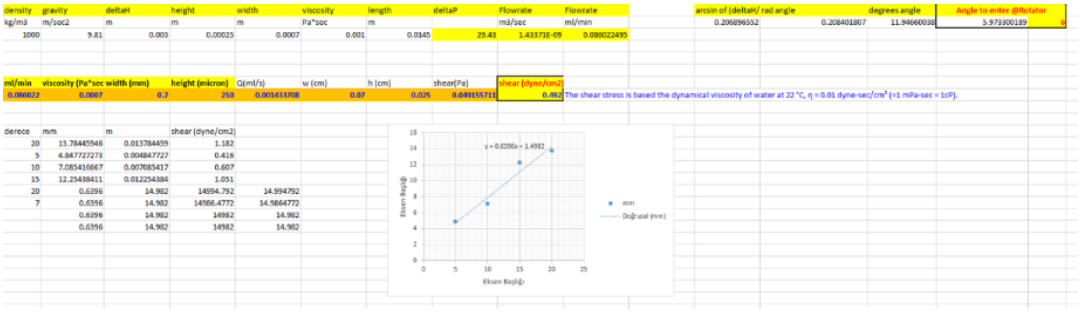

Figure A.6. Excel sheet showing shear stress calculation based on height, flow rate and height differences between inlet and outlet according to degree entered.

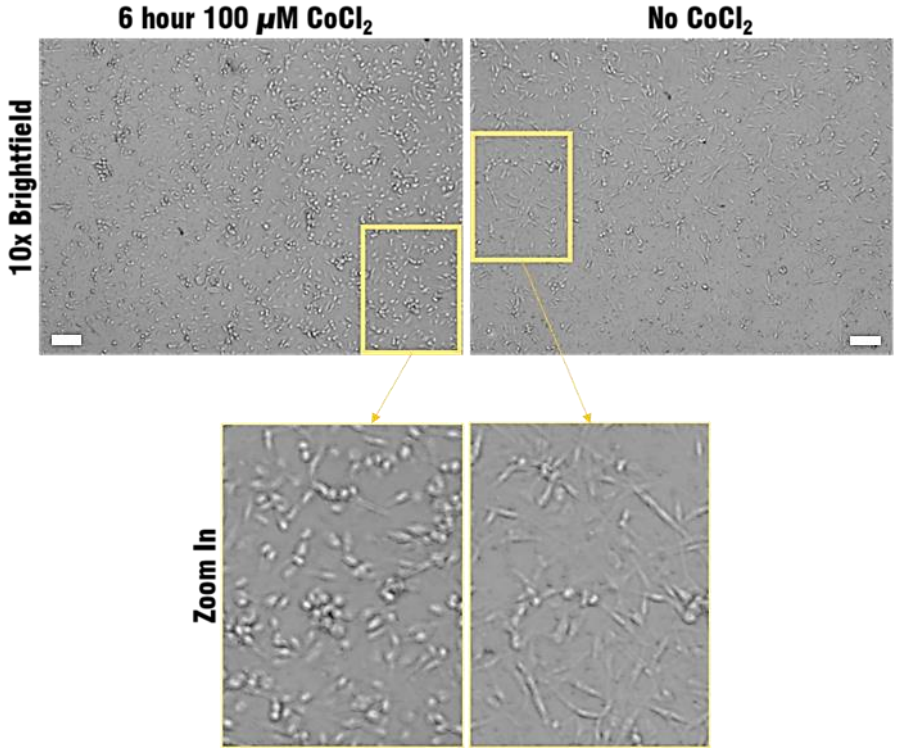

Figure A.7. Effect of 100 µM $CoCl_2$ treatment against MDAMB231 morphology. Scale bar: 100µm

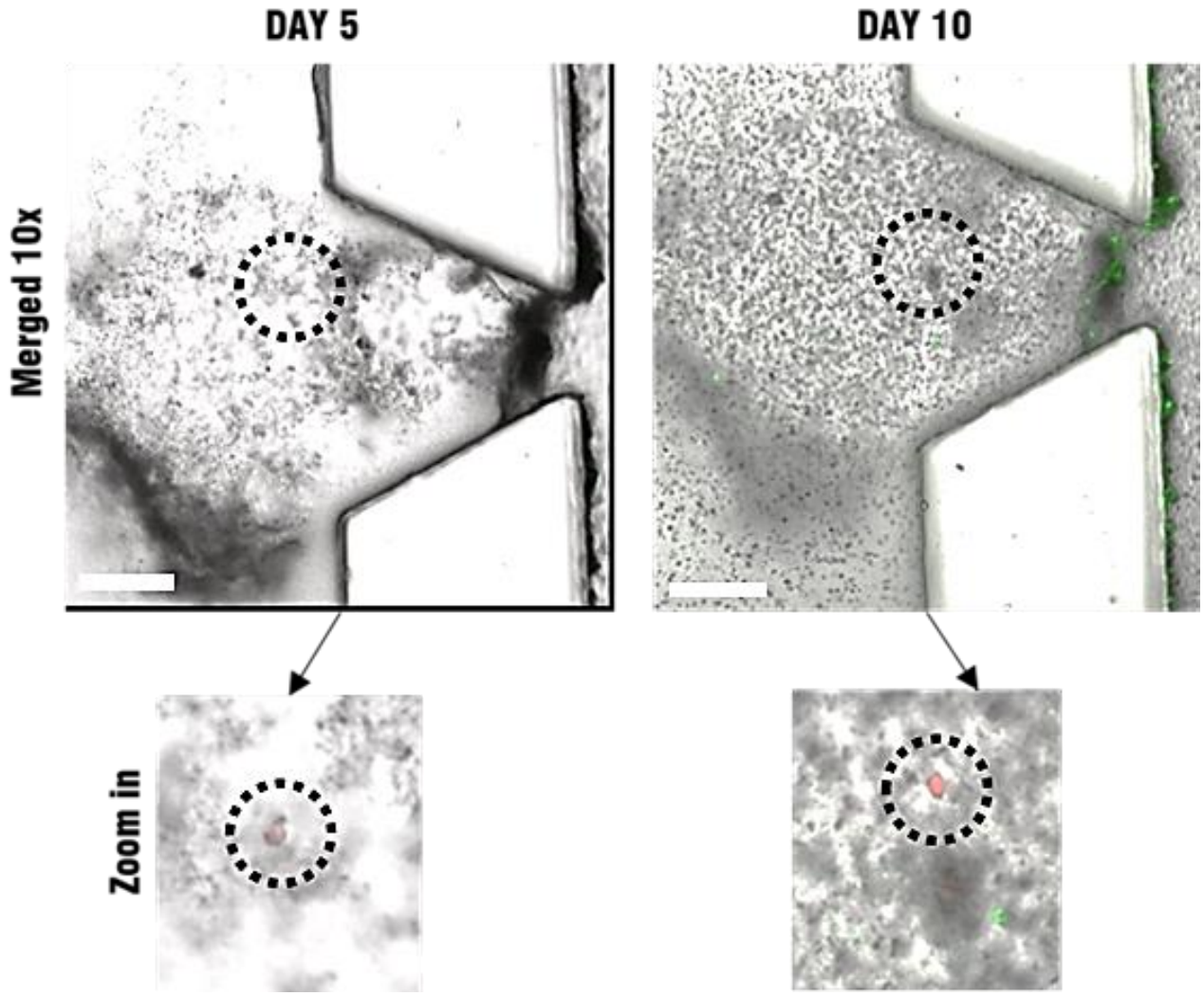

Figure A.8. Observation of tumor formation on 5th and 10th day. Scale Bar:200 μm

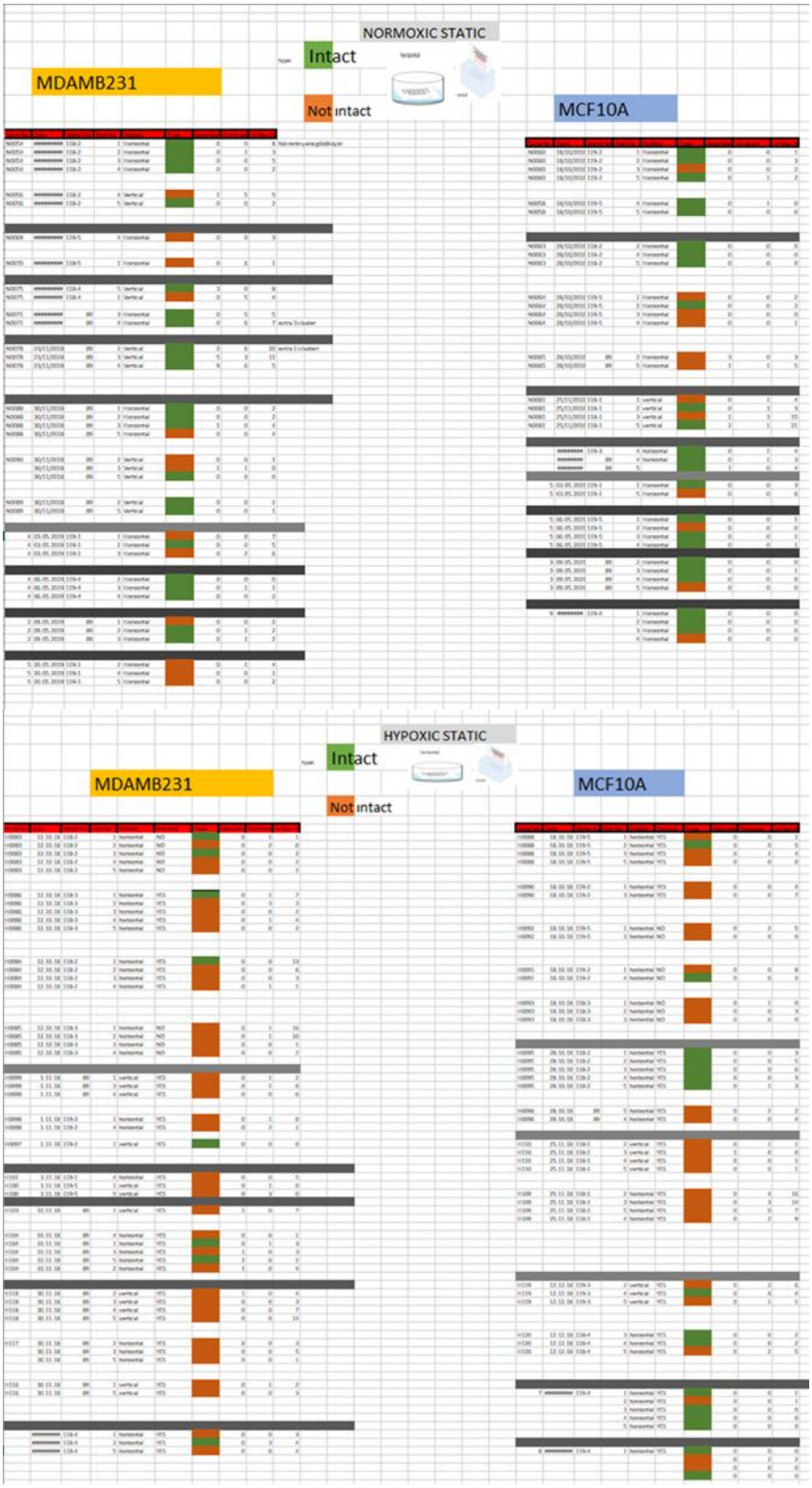

Figure A.**9.** Excel sheet showing extravasated, associated and total cells in flow channel according to hypoxic and normoxic situations without perfusion flow. green bar:intact monolayer, orange bar: nonintact monolayer.